Cell Reports

Article

An amygdala-to-cingulate cortex circuit for conflicting choices in chronic pain

Graphical abstract

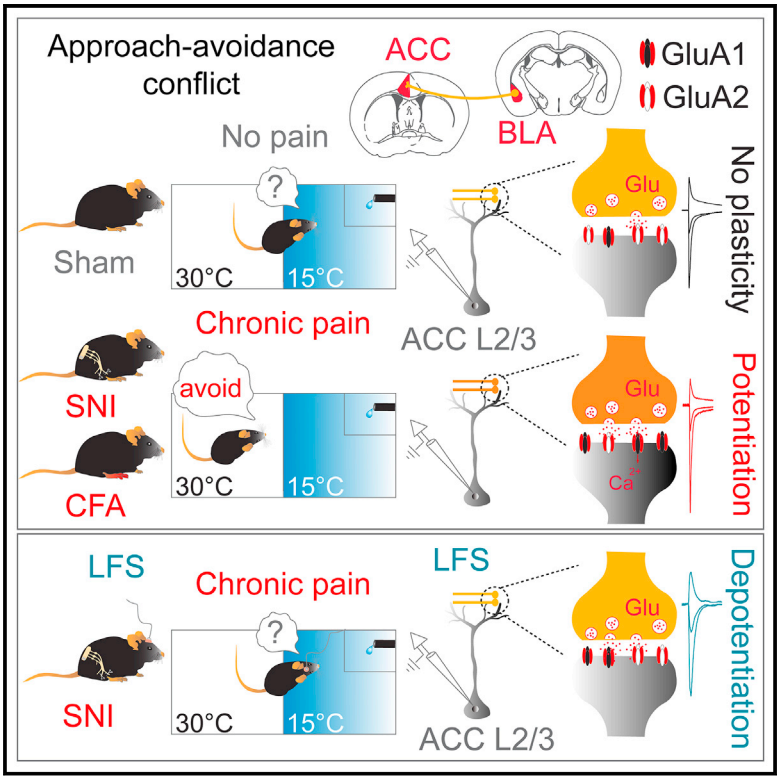

Highlights

- Mice with neuropathy and inflammatory pain favor cold avoidance in a conflicting task
- AMPAR transmission at BLA-ACC synapses in neuropathic animals is potentiated
- BLA-ACC circuit is necessary and sufficient for conflicting cold avoidance
- LFS of BLA-ACC projection restores AMPAR function and reduces avoidance

Authors

Kristina Valentinova, Mario A. Acuña, Niels R. Ntamati, Natalie E. Nevian, Thomas Nevian

Correspondence

kristina.valentinova@unibe.ch (K.V.), thomas.nevian@unibe.ch (T.N.)

In brief

Valentinova et al. describe that chronic pain mice display cold avoidance in approach-avoidance conflict. The pain state triggers AMPAR-mediated potentiation at amygdala-cingulate synapses (BLA-ACC). This circuit is required for pain-associated cold avoidance and is sufficient to induce cold avoidance in pain-free animals. Finally, low-frequency stimulation of BLA-ACC restores AMPAR function and reduces avoidance.

Valentinova et al., 2023, Cell Reports *42*, 113125
October 31, 2023
https://doi.org/10.1016/j.celrep.2023.113125

CellPress

Cell Reports

CellPress
OPEN ACCESS

Article

An amygdala-to-cingulate cortex circuit for conflicting choices in chronic pain

Kristina Valentinova,[1,*] Mario A. Acuña,[1] Niels R. Ntamati,[1] Natalie E. Nevian,[1] and Thomas Nevian[1,2,*]
[1]Department of Physiology, University of Bern, Bühlplatz 5, 3012 Bern, Switzerland
[2]Lead contact
*Correspondence: kristina.valentinova@unibe.ch (K.V.), thomas.nevian@unibe.ch (T.N.)
https://doi.org/10.1016/j.celrep.2023.113125

SUMMARY

Chronic pain is a complex experience with multifaceted behavioral manifestations, often leading to pain avoidance at the expense of reward approach. How pain facilitates avoidance in situations with mixed outcomes is unknown. The anterior cingulate cortex (ACC) plays a key role in pain processing and in value-based decision-making. Distinct ACC inputs inform about the sensory and emotional quality of pain. However, whether specific ACC circuits underlie pathological conflict assessment in pain remains underexplored. Here, we demonstrate that mice with chronic pain favor cold avoidance rather than reward approach in a conflicting task. This occurs along with selective strengthening of basolateral amygdala inputs onto ACC layer 2/3 pyramidal neurons. The amygdala-cingulate projection is necessary and sufficient for the conflicting cold avoidance. Further, low-frequency stimulation of this pathway restores AMPA receptor function and reduces avoidance in pain mice. Our findings provide insights into the circuits and mechanisms underlying cognitive aspects of pain and offer potential targets for treatment.

INTRODUCTION

Pain is a subjective sensory and emotional experience with both adaptive and pathological dimensions. When acute pain becomes chronic, it involves long-lasting brain network remodeling.[1] In the long run, this leads to dysfunctional behaviors, such as the inability to cope with stress, diminished cognitive and attentional abilities, and often depression, altogether contributing to the inherent pain unpleasantness and emotional burden.[2] The development of chronic pain is intrinsically bound to negative emotional states that result from the experience itself but also lead to a self-perpetuating cycle of suffering.[3] Indeed, pain catastrophizing is a characteristic tendency of individuals with chronic pain conditions to cognitively amplify the experience of actual and anticipated pain, which can transform into pain-related fears and anxiety.[4–6] These maladaptive states result in excessive avoidance behaviors, often at the expense of reward seeking, a behavioral framework known as the fear-avoidance model.[6] Particularly, in conflicting situations where valued life activities require effort (e.g., exercising despite the pain), favoring avoidance over approach often exacerbates the pain experience and dramatically impacts recovery.[3,6–9] Indeed, catastrophizing predicts the severity of the experienced pain as well as poor response to pain management.[10–12] Therefore an in-depth understanding of the brain mechanisms leading to such maladaptive responses is urgently needed.

Accumulating evidence suggests that the anterior cingulate cortex (ACC) is critically involved in the affective component of pain.[13] Indeed, the ACC is activated by nociceptive stimuli, shows aberrant activity in patients and animal models of chronic pain,[14–18] and is associated with pain unpleasantness.[19] Furthermore, specific ACC activity patterns predict the onset of pain avoidance.[20] Additionally, the ACC plays a pivotal role in assessing mixed outcomes when appetitive and aversive stimuli are present together and guides goal-directed behaviors.[21] Indeed, as an associative area, the ACC orchestrates adaptive responses such as value-based action selection and decision-making.[22,23] Altogether, this makes the ACC a hub for processing the emotional, sensory, and cognitive aspects of pain and suggests that maladaptive mechanisms taking place within the ACC may underlie aspects of pain behaviors. The ACC receives inputs from different sensory, limbic, and cortical brain regions, distinctly contributing to pain behaviors. Indeed, inputs from the mediodorsal thalamus and the somatosensory cortex have been shown to exacerbate pain-related aversion,[24–26] while an input from the parafascicular thalamic nucleus plays a role in depression-induced allodynia.[27] However, the circuits involved in maladaptive conflict assessment and excessive avoidance behaviors observed in pain conditions remain unknown. Importantly, the basolateral amygdala (BLA), a key structure orchestrating fear and anxiety,[28] mediates behavioral selection in approach-avoidance conflicts mainly via its projections to the prefrontal cortex (PFC).[29] Moreover the BLA encodes nociceptive stimuli and underlies motivational aspects of pain.[30,31] However, whether a BLA-ACC circuit contributes to pain-related avoidance behaviors remains elusive.

Here, we hypothesize that BLA projections to the ACC undergo plasticity in chronic pain states contributing to pain-withdrawal behaviors. We find that animals with neuropathy or inflammatory pain display cold avoidance in a conflicting approach-avoidance

task (CAAT), while reward approach in the absence of aversive stimuli or cold avoidance in the absence of rewarding stimuli remain unchanged. We further show synaptic strengthening of BLA inputs to ACC layer 2/3 (L2/3) pyramidal, but not to L5 pyramidal or interneurons in neuropathic animals. This involves an increased contribution of α-amino-3-hydroxy-5-methyl-4-isoxazolepropionic acid receptors (AMPARs) that are Ca^{2+} permeable and lack the GluA2 subunit. Additionally, chemogenetic activation of the BLA-ACC pathway is sufficient to induce cold avoidance in pain-free mice. Low-frequency stimulation (LFS) of BLA projections to ACC L2/3 *ex vivo* reduces synaptic strength and rebalances AMPAR subunit composition. Finally, chemogenetic inhibition or LFS of the BLA-ACC circuit *in vivo* reduces neuropathic animals' cold avoidance in the conflicting task.

RESULTS

Chronic pain facilitates avoidance when facing approach-avoidance choices

We used the spared nerve injury (SNI) model of neuropathic pain (Figure 1A) and first characterized different sensory and motivational behaviors (Figure 1B). As previously shown,[32] SNI mice displayed long-lasting mechanical allodynia (Figure 1C) and coping behavior in response to hot water or an acetone (cold) drop applied on the injured hind paw, indicative of thermal allodynia (Figure 1D). However, when allowed to explore a linear thermal gradient track with temperature zones spanning from 8°C to 46°C, all mice had similar preference for the comfortable range (between 24°C and 34°C) and similar avoidance of the extreme temperatures (Figure S1A). Altogether, these results suggest that neuropathic mice have higher thermal sensitivity compared to control animals but similar thermal avoidance when granted free choice. We also tested sham and SNI mice's motivation for an appetitive stimulus using the sucrose preference test. Both groups displayed a similar preference for the sucrose solution, indicating the absence of anhedonia (Figure S1B). Collectively, these data suggest that, at least at this time point after surgery (6 weeks post-operation), both groups have similar avoidance or approach behaviors when facing aversive or appetitive stimuli, respectively.

In order to investigate the idea that chronic pain shifts behavioral choices toward pain avoidance rather than reward approach when both appetitive and aversive stimuli are present together, we designed a CAAT in which animals were given the opportunity to consume a reward but in an aversive environment. The task consisted of a training phase and a test phase, followed by a thermal place avoidance task. During the 7-day training phase, sham and SNI mice were exposed for 15 min each day to a two-compartment arena with 30°C floor temperature. All animals were allowed to lick from a water spout delivering sucrose solution (10%) positioned in one of the compartments. Both groups developed similar preference (~60% of the time) for the sucrose-associated compartment, spending ~40% of the total duration specifically in the licking zone (Figures 1E and 1F) and consumed similar amounts of sucrose (Figure 1G), confirming that in the absence of conflict, both groups display reward approach. During the test phase, a conflict was introduced. Indeed, the floor of the sucrose-associated compartment was set to either 45°C or 15°C, while the other one remained at 30°C, and therefore the animals had to consume the reward in an unpleasant thermal environment. We reasoned that the absolute value of the rewarding and the aversive stimuli should be approximately equal so that animals could have relatively balanced approach and avoidance behaviors, hence the choice of aversive but not extreme temperatures. In this conflicting situation, all animals spent less time in the sucrose compartment compared with the training phase; however, SNI mice showed lower preference compared with sham mice when the floor was cold but not when it was hot (Figures 1K and 1H). Notably, sham and SNI mice spent similar but low amounts of time in the lick zone during the hot conflict (Figure 1I). However, SNI mice consumed less sucrose solution (Figure 1J), suggesting that despite the averseness of the hot temperature for both groups, SNI mice display lower motivation for the reward. Conversely, the time SNI mice spent in the lick zone during the cold conflict as well as their sucrose consumption were significantly lower than those of sham mice (Figures 1L and 1M), further supporting that in a conflicting situation, animals with chronic pain are less motivated for a reward and instead favor avoidance. Importantly, no differences in mobility were observed between groups during the total duration of the test (Figure S1C). Furthermore, in a passive thermal place preference (TPP) task, where animals were exposed to the same arena but in the absence of reward, sham and SNI mice displayed similar avoidance of the aversive compartment (45°C or 15°C) (Figures S1D and S1E).

We further assessed whether this approach-avoidance conflict behavior is also present in animals with acute pain and whether it is specific for neuropathy. We used an acute and prolonged inflammatory pain model, induced by an injection of the inflammatory agent complete Freund's adjuvant (CFA) in the left hind paw of mice (Figure S2A). This led to mechanical allodynia of CFA-injected mice in the acute (24 h) and prolonged (1 week) phases after injection (Figure S2B) as well as to thermal allodynia 1 week post-injection (Figure S2C). We performed the conflicting task by first exposing naive mice to the training phase, where all animals had free access to the sucrose solution in a comfortable temperature setting. All animals developed preference for the sucrose compartment over the training days and spent ~40% of the total time in the licking zone (Figure S2D). On the last day of the training (day 7), half of the animals were injected with saline and the other half with CFA in the left hind paw just prior to exposing them to the arena. Importantly, the injection of CFA did not affect their preference (Figure S2E) or the sucrose consumption (Figure S2F) as compared with the previous day when animals were injection naive. However, the CFA injection did reduce animals' mobility on day 7 (Figure S2M). The hot and cold tests were performed 24 and 48 h after injection, respectively, to assess the effect of acute inflammation, and 1 week after, to assess the long-term effect of the inflammation. We did not observe differences in the preference score during the hot test between saline and CFA groups 24 h or a week after injection (Figure S2G), as indicated also by their similar time spent in the licking zone (Figure S2H). Interestingly, both groups displayed lower preference scores for the hot compartment 1 week after injection compared with 24 h after, but CFA mice

CellPress
OPEN ACCESS

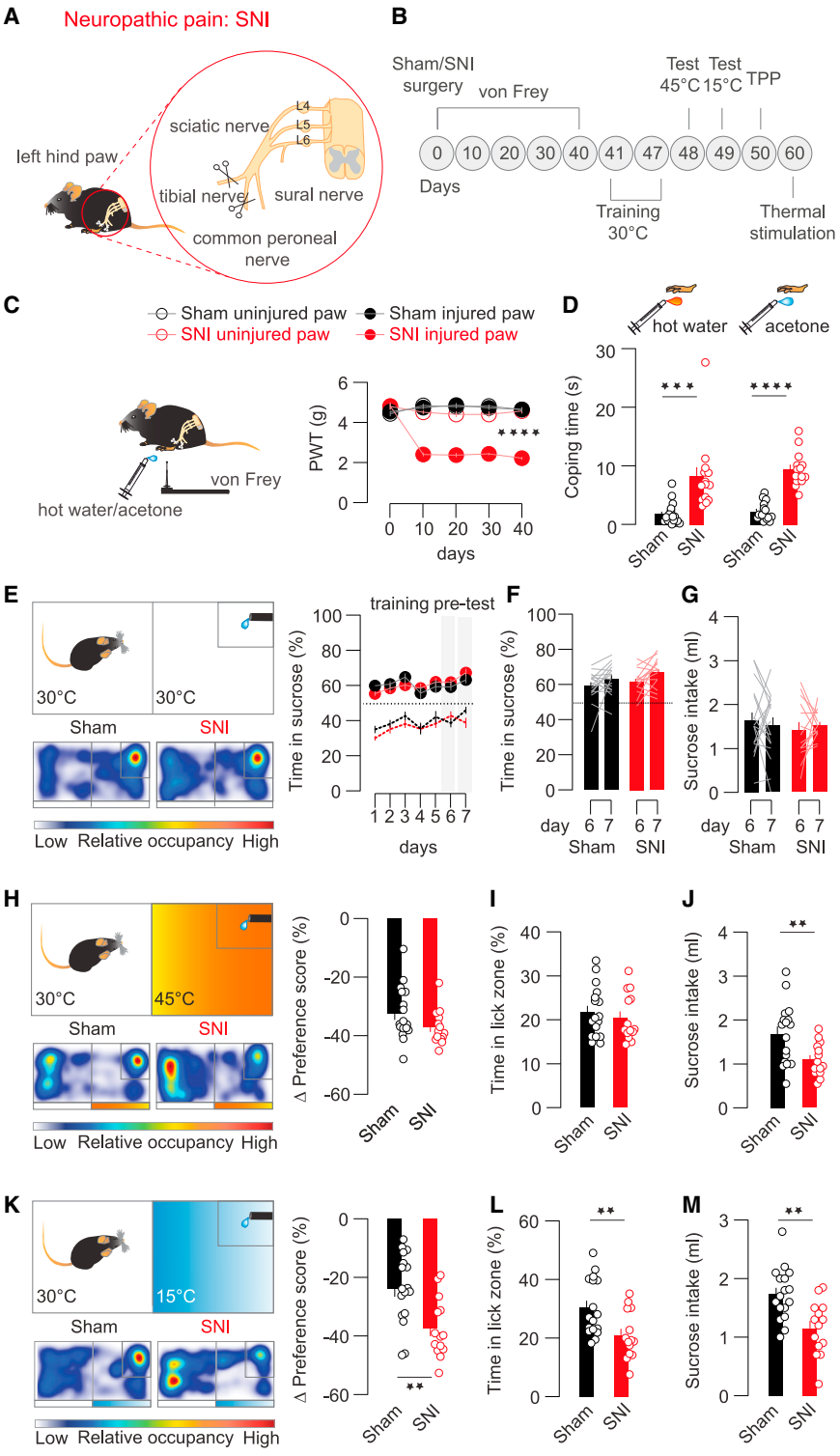

Figure 1. SNI mice display mechanical and thermal allodynia as well as cold avoidance in a conflicting approach-avoidance task

(A) Schematic of SNI surgery. The peroneal and tibial branches of the sciatic nerve were cut and ligated, while the sural was spared.

(B) Timeline of surgeries and behavioral experiments. TPP, thermal place preference.

(C) Left: schematic of mechanical and thermal stimulations of the injured paw of sham (black) and SNI (red) mice. Right: von Frey test measuring the paw withdrawal threshold (PWT; in grams) of the injured (filled circles) and uninjured paws (empty circles) before and 10, 20, 30, and 40 days after surgery (N = 17 vs. 14 mice, two-way ANOVA, interaction $F_{(12, 290)} = 23.79$, ****$p < 0.0001$).

(D) Affective coping following hot water and acetone drop applied on the injured paw of sham and SNI (hot water; N = 17 vs. 14 mice, 1.91 ± 0.45 s vs. 8.27 ± 1.64 s, unpaired t test, $t_{29} = 4.068$, ***$p = 0.0003$; acetone; N = 17 vs. 14 mice, 2.42 ± 0.37 s vs. 9.49 ± 0.78 s, unpaired t test, $t_{29} = 8.656$, ****$p < 0.0001$).

(E) Left: training phase of the CAAT and heatmaps showing the relative time spent in the 30°C and 30°/sucrose compartments for sham and SNI mice. Right: percentage of time spent in the sucrose compartment (thick lines with circles) and in the licking zone of the sucrose compartment (dashed lines) during the 7-day training (N = 17 vs. 14 mice, two-way ANOVA, interaction $F_{(18,406)} = 0.92$, $p = 0.553$). The last 2 days (pre-test) were used to calculate the average baseline preference for the sucrose-associated compartment.

(F) Percentage of time spent in the sucrose compartment in the last 2 days of the training (sham: N = 17 mice, day 6 vs. 7: 59.13% ± 2.12% vs. 63.39% ± 2.07%, paired t test, $t_{16} = 1.603$, $p = 0.129$; SNI: N = 14 mice, day 6 vs. 7: 61.89% ± 1.95% vs. 67.25% ± 2.25%, paired t test, $t_{13} = 2.058$, $p = 0.06$).

(G) Sucrose intake in the last 2 days of the training (sham: N = 17 mice, day 6 vs. 7: 1.63 ± 0.19 mL vs. 1.52 ± 0.18 mL, paired t test, $t_{16} = 0.53$, $p = 0.61$; SNI: N = 14 mice, day 6 vs. 7: 1.40 ± 0.18 mL vs. 1.51 ± 0.08 mL, paired t test, $t_{13} = 0.59$, $p = 0.56$).

(H) Left: hot test of the CAAT and heatmaps showing the relative time spent in the 30°C and 45°C/sucrose compartments for sham and SNI mice. Right: difference of time spent in the 45°C/sucrose compartment from baseline (N = 17 vs. 14 mice, −32.42% ± 2.20% vs. −37.15% ± 1.57%, unpaired t test, $t_{29} = 1.684$, $p = 0.1$).

(I) Percentage of time spent in the lick zone of the 45°C/sucrose compartment (N = 17 vs. 14 mice, 21.73% ± 1.4% vs. 20.41% ± 1.43%, unpaired t test, $t_{29} = 0.66$, $p = 0.52$).

(J) Sucrose intake during hot conflict (N = 17 vs. 14 mice, 1.69 ± 0.17 mL vs. 1.10 ± 0.1 mL, unpaired t test, $t_{29} = 2.84$, **$p = 0.008$).

(K) Same as in (H) but for the cold test (N = 17 vs. 14 mice, −23.69% ± 2.9% vs. −37.41% ± 2.68%,unpaired t test, $t_{29} = 3.413$, **$p = 0.002$).

(L) Same as in (I) but for the cold test (N = 17 vs. 14 mice, 30.43% ± 2.34% vs. 21.04% ± 2.17%, unpaired t test, $t_{29} = 2.89$, **$p = 0.007$).

(M) Same as in (J) but for the cold test (N = 17 vs. 14 mice, 1.73 ± 0.11 mL vs. 1.16 ± 0.12 mL, unpaired t test, $t_{29} = 3.54$, **$p = 0.0014$).

Data are presented as mean ± SEM.

See also Figures S1 and S2.

had lower sucrose intake than saline mice at this time point (Figure S2I). Different were the results with the cold temperature. Although we did not observe differences in the acute phase of the test (48 h post-injection), CFA mice had a lower preference score a week following injection (Figure S2J), spent less time in the lick zone (Figure S2K), and consumed less sucrose solution (Figure S2L). This avoidance behavior of CFA mice occurred regardless of their higher mobility a week after injection (Figure S2M) and was not associated with differential avoidance of the hot or cold compartment in a passive TPP task in the absence of reward (Figures S2N and S2O).

Altogether, these results demonstrate that, indeed, different types of chronic, but not acute, pain represent aspects of the human pain-avoidance behavior when facing conflicting choices. Importantly, this conflict-related avoidance was particularly present when a cold temperature was used as aversive signal.

Neuropathic pain selectively drives plasticity at BLA inputs to L2/3 pyramidal neurons in the ACC

Activity in the ACC underlies negative affective states in chronic pain[33] and in conflict evaluation.[34] Importantly, distinct thalamic, cortical, and limbic inputs drive neuronal activity across ACC layers,[35,36] and their contribution to specific aspects of pain behaviors has been increasingly reported.[17,24–26] Accumulating evidence suggests a pivotal role of the ACC and the BLA in cost-benefit decision-making[37] as well as in negative states associated with pain and fear.[31,38] The BLA is reciprocally connected to the ACC and has been involved in pain processing and conflicting behaviors. Particularly, activity of the BLA projection to the PFC shifts behavioral selection toward negative outcomes,[29] and BLA neuronal activity underlies affective states in pain.[30,39] To test the implication of a BLA-ACC circuit in pain-induced avoidance behaviors, we first characterized the anatomical connectivity and synaptic properties of this projection in the SNI model. We performed rabies-based input-mapping in the ACC and showed monosynaptic projections from the BLA to pyramidal neurons (Figure S3). To determine whether neuropathic pain leads to synaptic changes at BLA inputs to the ACC, we first expressed an excitatory opsin (AAV2-CaMKII-ChR2) in the BLA of sham- and SNI-operated mice. We performed voltage-clamp recordings from identified L2/3 or L5 pyramidal or GABA neurons in ACC-containing acute slices to assess pre- and post-synaptic strength in response to BLA input stimulation (Figure 2A). BLA axons distributed throughout L2/3 and L5 of the ACC, with the highest density in L2/3 (Figure 2B). We first measured the excitatory AMPAR- and inhibitory γ-aminobutyric acid type A receptor (GABAaR)-mediated post-synaptic currents (EPSCs and IPSCs, respectively) upon BLA input stimulation in L2/3 pyramidal neurons (Figure 2C). The corresponding AMPA/GABA ratios were comparable between neurons obtained from sham and SNI mice (Figure 2D). Moreover, AMPA/GABA ratios did not change between groups when recorded from L5 pyramidal or interneurons of the ACC (Figures S4A, S4B, S4G, and S4H), suggesting that no major changes of the excitation-inhibition balance occur at BLA synapses in the ACC of neuropathic animals. We further assessed the strength of excitatory transmission by measuring AMPA/NMDA (N-methyl-D-aspartate) ratios across ACC layers. We performed voltage-clamp recordings of the AMPAR-mediated component either at −70 or 40 mV to detect potential voltage-dependent modifications of these receptors. We found a reduced AMPA/NMDA ratio only in L2/3 pyramidal neurons, but not L5 pyramidal or GABA neurons, in slices from SNI mice when both components were measured at positive potential (Figures 2E, S4C, and S4I). However, when AMPAR-mediated currents were measured at negative (−70 mV) potential, we did not observe significant changes of excitatory strength in any of the assessed cell types (Figures 2F, S4D, and S4J). Such discrepancies of AMPAR function at different potentials could result from modifications of their biophysical properties, for example a switch of their composing subunits, rendering them less conductive at positive membrane potentials.[40] To test this scenario, we performed recordings of pharmacologically isolated AMPAR-EPSCs at positive and negative potentials and measured the current-voltage relationships. This allowed us to compute an AMPAR rectification index for BLA synapses in the ACC, a property dependent on their specific subunit composition. We found higher AMPAR rectification properties when recording from ACC L2/3 pyramidal neurons of SNI mice compared with the sham controls (Figure 2G) but no modifications in L5 pyramidal or GABA neurons (Figures S4E and S4K). These results indicate that AMPARs at these SNI L2/3 synapses may have higher expression of the inwardly rectifying Ca^{2+}-permeable and GluA2-lacking AMPARs. To test this idea, we applied the selective antagonist of these receptors 1-naphthylacetyl spermine trihydrochloride (NASPM; 20 μM) to measure their relative contribution to the total AMPAR-EPSC in slices from sham and SNI mice. We found indeed a larger decrease of AMPAR-EPSC amplitude following the drug application in SNI slices (Figure 2H), confirming that the pain state involves synapse-specific AMPAR adaptations. These findings are consistent with previous reports[41] and are supported by the high relevance of these receptors for the expression of experience-dependent plasticity.[42] We also assessed presynaptic release at BLA-L2/3, L5, and GABA neurons synapses. Notably, we observed increased paired-pulse depression only at BLA-L2/3 pyramidal neurons (Figure 2I), indicating higher release probability, but no differences at BLA-L5 pyramidal or GABA neurons (Figures S4F and S4L). Altogether, we find pain-induced synaptic potentiation specifically at BLA inputs to L2/3 pyramidal neurons.

The BLA-ACC circuit is required for pain-associated cold avoidance in approach-avoidance conflict

Given the potentiated state of BLA-ACC synapses in neuropathic pain, we asked whether reducing the activity of BLA-ACC projections would impact the behavior of neuropathic animals. To this end, we employed a chemogenetic strategy by bilaterally injecting a retro-Cre virus in the ACC and a Cre-dependent Gi-coupled inhibitory designer receptor exclusively activated by designer drugs (DREADDi; hM4Di) or a control virus in the BLA (Figure 3A). We first tested whether expression of hM4Di in ACC-projecting BLA neurons affects their activity and physiological properties. We recorded their firing rate in response to current step injections as well as the resting membrane potential (Vm) and input resistance (Ri) before and after application of the DREADDi agonist clozapine-N-oxide (CNO). Indeed, CNO reduced the firing rate as well as Vm and Ri of hM4Di-positive neurons in the BLA (Figures S5A–S5D). We next assessed if inhibition of BLA

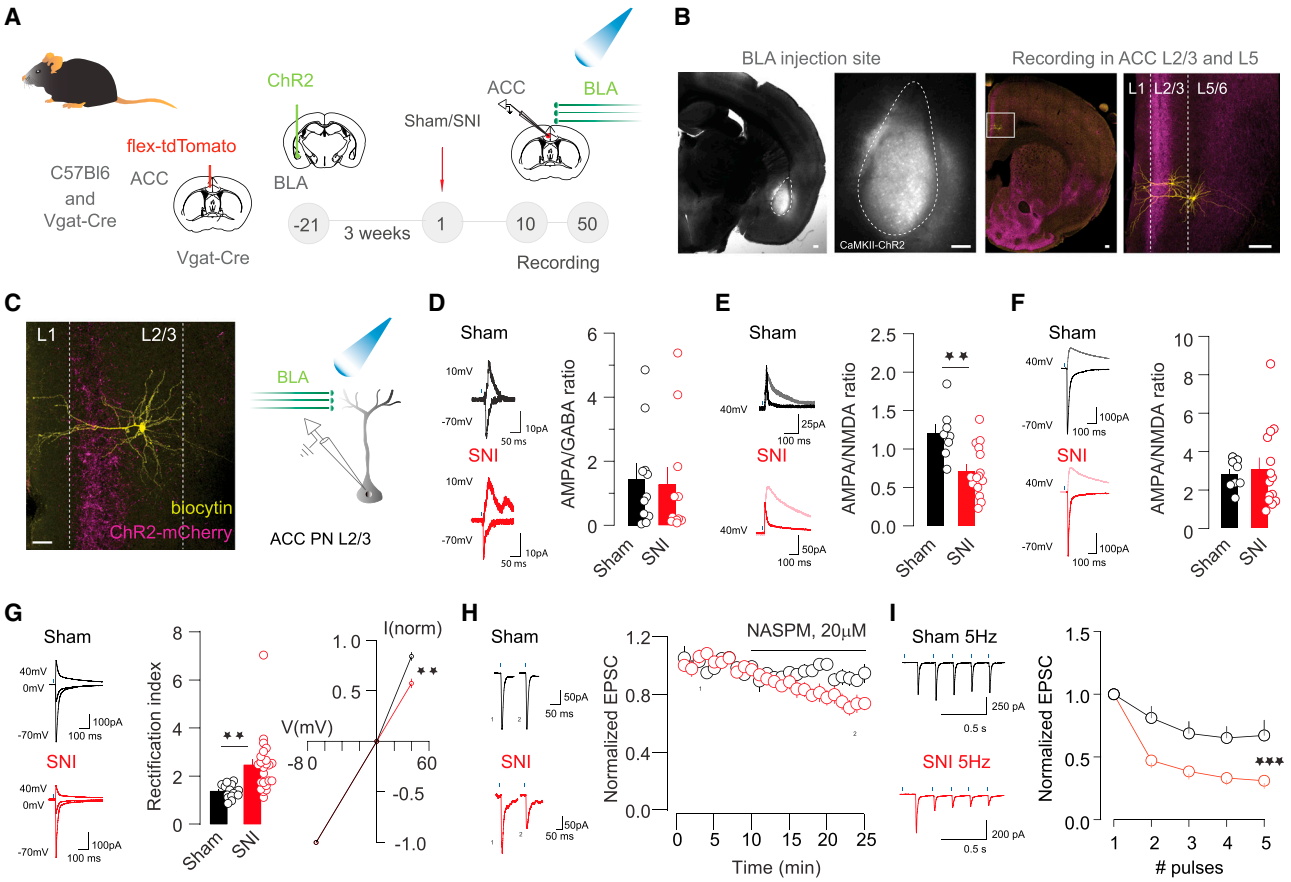

Figure 2. Neuropathy-induced potentiation of excitatory transmission selectively at BLA inputs onto ACC layer 2/3 pyramidal neurons

(A) Schematic of viral injections, sham/SNI surgeries, and recordings. Vgat-Cre mice were used for interneuron-targeted recordings.

(B) Example images showing ChR2 expression in BLA neurons and ChR2-positive terminals in the ACC. Scale bars: 100 μm.

(C) Left: example image showing a biocytin-filled L2/3 pyramidal neuron (PN). Scale: 50 μm. Right: schematic of L2/3 PN recordings in response to BLA terminal stimulation.

(D) Example traces and AMPA/GABA ratios from ACC L2/3 PNs of sham and SNI brain slices (N = 5 vs. 7 mice, n = 11 vs. 11 cells, 1.45 ± 0.47 vs. 1.28 ± 0.55, unpaired t test, $t_{20} = 0.238$, p = 0.81). Blue bar indicates the stimulation.

(E) Example traces and AMPA/NMDA ratios (obtained at 40 mV) from ACC L2/3 PNs of sham and SNI mice brain slices (N = 5 vs. 10 mice, n = 8 vs. 15 cells, 1.21 ± 0.12 vs. 0.71 ± 0.08, unpaired t test, $t_{21} = 3.44$, **p = 0.0025).

(F) Example traces and AMPA/NMDA ratios (measured at −70 and 40 mV) from ACC L2/3 PNs of sham and SNI mice (N = 5 vs. 9 mice, n = 8 vs. 14 cells, 2.79 ± 0.27 vs. 3.08 ± 0.57, unpaired t test, $t_{20} = 0.37$, p = 0.716).

(G) Left: example traces of AMPAR EPSCs obtained at −70, 0, and 40 mV and the corresponding rectification index from ACC L2/3 PNs of sham and SNI slices (N = 7 vs. 11 mice, n = 14 vs. 23 cells, 1.36 ± 0.08 vs. 2.46 ± 0.25, unpaired t test, $t_{35} = 3.352$, **p = 0.0019). Right: normalized and liquid-junction potential-corrected current-voltage relationship curve (I/V) showing AMPAR rectification properties.

(H) Example traces and time plot showing the effect of NASPM (20 μM) on AMPAR-EPSCs recorded in ACC L2/3 PNs from sham and SNI brain slices (N = 3 vs. 7 mice, n = 7 vs. 11 cells, sham baseline vs. post-NASPM: 0.93 ± 0.03, paired t test: $t_6 = 2.57$, *p = 0.042; SNI baseline vs. post-NASPM: 0.75 ± 0.05, paired t test, $t_{10} = 4.539$, **p = 0.001; sham vs. SNI, unpaired t test, $t_{16} = 2.499$, *p = 0.024).

(I) Example traces and normalized EPSC vs. pulse number plot recorded at 5 Hz in ACC L2/3 PNs from sham and SNI slices (N = 5 vs. 5 mice, n = 8 vs. 11 cells, two-way ANOVA, interaction $F_{(4,85)} = 2.997$, *p = 0.023; effect of pain $F_{(1,85)} = 46.89$, ****p < 0.0001).

Data are presented as mean ± SEM.

See also Figures S3 and S4.

projections to the ACC affects mechanical and thermal allodynia. We first performed the von Frey test at different time points after surgery, and on day 40, all animals received a CNO injection prior to testing. This manipulation did not affect the mechanical allodynia of SNI mice (Figure S6A). We also performed hot and cold stimulations of the injured paw before and after CNO injection and measured the animal's coping behavior. Similarly, we did not observe any changes in this behavior upon BLA-ACC inhibition (Figure S6B), suggesting that this circuit is not required for the mechanical and thermal allodynia of SNI mice. We further tested whether BLA-ACC inhibition ameliorates SNI mice's performance in the CAAT. Sham and SNI mice expressing either hM4Di or a control virus in ACC-projecting BLA neurons underwent habituation to the arena as described above and developed

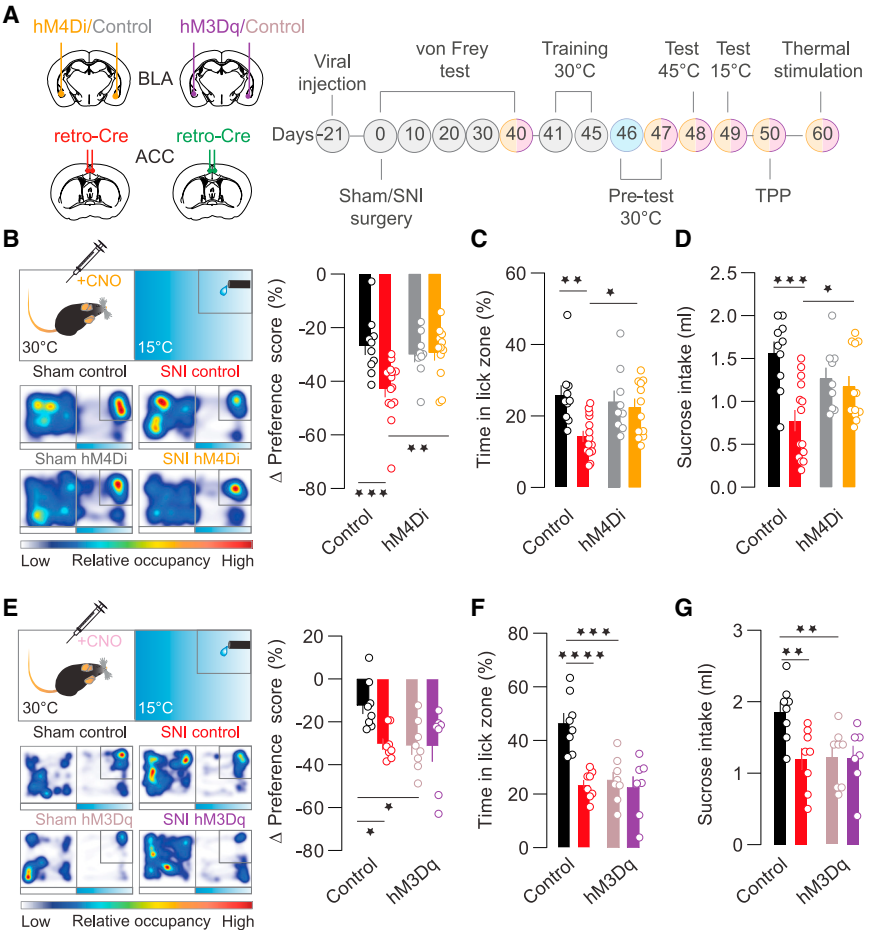

Figure 3. Inhibition of ACC-projecting BLA neurons reduces SNI animal's cold avoidance in the conflicting task, while their activation triggers it in pain-free mice

(A) Schematics and timeline of viral injections, surgeries, and behavioral experiments. The orange-purple shading indicates CNO injection, and the blue shading indicates saline injection.

(B) Left: cold test of the CAAT and heatmaps showing the relative time spent in the 30°C and sucrose/15°C compartments for sham-control (black), SNI-control (red), sham-hM4Di (gray), and SNI-hM4Di (orange) mice after receiving CNO injection. Left: difference of preference for the sucrose/15°C compartment from baseline preference (N = 10 vs. 14 vs. 9 vs. 12 mice, −26.74% ± 3.42% vs. −42.96% ± 2.95% vs. −29.97% ± 2.84% vs. −29.32% ± 2.89%, two-way ANOVA, interaction $F_{(1,41)}$ = 7.37, **p = 0.0097, Sidak's multiple comparison: sham-control vs. SNI-control ***p = 0.0009, SNI-control vs. SNI-hM4Di **p = 0.003).

(C) Percentage of time spent in the lick zone of the cold compartment (N = 10 vs. 14 vs. 9 vs. 12 mice, 25.81% ± 2.82% vs. 14.33% ± 1.53% vs. 24.04% ± 3.05% vs. 22.01% ± 2.2%, two-way ANOVA, interaction $F_{(1,41)}$ = 4.082, *p = 0.049; Sidak's multiple comparison: sham-control vs. SNI-control **p = 0.0018, SNI-control vs. SNI-hM4Di *p = 0.03).

(D) Sucrose intake during cold conflict (N = 10 vs. 14 vs. 9 vs. 12 mice, 1.57 ± 0.13 mL vs. 0.78 ± 0.12 mL vs. 1.27 ± 0.13 mL vs. 1.17 ± 0.12 mL, two-way ANOVA, interaction $F_{(1,41)}$ = 7.34, **p = 0.0098; Sidak's multiple comparison: sham-control vs. SNI-control ***p = 0.0001, SNI-control vs. SNI-hM4Di *p = 0.044).

(E) Left: cold test of the CAAT and heatmaps showing the relative time spent in the 30°C and sucrose/15°C compartments for sham-control (black), SNI-control (red), sham-hM3Dq (rose), and SNI-hM3Dq (purple) mice after receiving CNO injection. Left: difference of preference for the sucrose/15°C compartment from baseline (N = 8 vs. 8 vs. 8 vs. 7 mice, −12.31% ± 4.04% vs. −30.39% ± 2.60% vs. −31.22% ± 4.11% vs. −31.36% ± 7.16%, two-way ANOVA, interaction $F_{(1,27)}$ = 3.83, p = 0.061, Sidak's multiple comparison: sham-control vs. SNI-control *p = 0.017, sham-control vs. Sham-hM3Dq *p = 0.012).

(F) Percentage of time spent in the lick zone of the cold compartment (N = 8 vs. 8 vs. 8 vs. 7 mice, 46.56% ± 3.72% vs. 23.51% ± 1.82% vs. 25.30% ± 2.93% vs. 22.54% ± 4.11%, two-way ANOVA, interaction $F_{(1,27)}$ = 9.97, **p = 0.004; Sidak's multiple comparison: sham-control vs. SNI-control ****p < 0.0001, sham-control vs. Sham-hM3Dq ***p = 0.0001).

(G) Sucrose intake during cold conflict (N = 8 vs. 8 vs. 8 vs. 7 mice, 1.86 ± 0.14 mL vs. 1.2 ± 0.15 mL vs. 1.23 ± 0.14 mL vs. 1.22 ± 0.16 mL, two-way ANOVA, interaction $F_{(1,27)}$ = 4.88, *p = 0.036; Sidak's multiple comparison: sham-control vs. SNI-control **p = 0.007, sham-control vs. sham-hM3Dq **p = 0.0095).

Data are presented as mean ± SEM.

See also Figures S5–S8.

preference for the sucrose compartment during the first 5 days of the training (Figure S6C). On day 6, all animals received a saline injection and on day 7 a CNO injection prior to habituation. There was no significant effect of CNO on mice's preference for the sucrose compartment or on their sucrose consumption compared with the saline injection the day prior, indicating that inhibition of BLA-ACC connections does not affect the motivation of mice for an appetitive stimulus (Figures S6D and S6E). On the cold test day, the control virus-expressing SNI mice showed significantly lower preference scores for the sucrose compartment, spent less time in the lick zone, and consumed lower amounts of sucrose solution as compared with the sham controls. Conversely, hM4Di-expressing SNI mice had a preference score similar to the sham groups, spent more time in the lick zone, and had higher sucrose intake than SNI control virus-expressing mice (Figures 3B–3D). Interestingly, inhibition of BLA-ACC inputs increased slightly the preference score of SNI mice for the sucrose compartment when the floor was hot (45°C), although there was no difference between SNI and sham control virus groups (Figure S6F). Accordingly, all groups spent similarly low time in the lick zone of the hot compartment (~20%), although SNI control mice consumed less sucrose solution (Figures S6G and S6H). We excluded a mobility effect of BLA-ACC inhibition, as all animals traveled similar distances throughout the days of the test (Figure S8A). To assess whether the improvement in SNI animals' preference in the conflicting task upon BLA-ACC inhibition was due to a higher tolerance of hot or cold temperatures, all four groups received a CNO injection before being exposed to a

TPP task in the absence of reward. All mice displayed again similar avoidance of both the hot and the cold temperatures (Figures S6I and S6J). Altogether, these results indicate that reduction of BLA-ACC activity does not affect approach or avoidance behaviors alone but reduces pain-associated cold avoidance specifically in the face of conflict.

Activation of the BLA-ACC circuit is sufficient to induce conflicting cold avoidance in pain-free animals

In light of these findings, we next wondered whether BLA-ACC activity is sufficient to trigger avoidance even in the absence of pain. For this we used an excitatory DREADD (hM3Dq), which we expressed specifically in BLA neurons projecting to the ACC by using again a retro-Cre strategy (Figure 3A). We first tested the effect of a CNO injection on mechanical and thermal allodynia. We did not observe pain-like coping behaviors in hM3Dq-expressing sham animals or any further pain behaviors of hM3Dq-expressing SNI animals (Figures S7A and S7B). We then performed the conflicting task as described above. We validated that during the training phase, all animals developed preference for the sucrose-associated compartment (Figure S7C). We injected all groups with saline on day 6 and with CNO the day after, which did not affect the preference for the sucrose compartment or the sucrose intake of any of the groups (Figures S7D and S7E). During the cold test, we observed a decrease in the preference score, a lower time spent in the lick zone, and a lower sucrose intake of hM3Dq-expressing sham mice compared with the control virus-expressing ones, and there was no further decrease in hM3Dq-expressing SNI animals (Figures 3E–3G). These results indicate that BLA-ACC activation is sufficient to trigger cold avoidance in pain-free animals. Interestingly, this effect seems to be present only with cold, as we did not observe similar changes in the hot test, where sham-hM3Dq mice performed as the control virus-expressing sham group (Figures S7F–S7H). To further assess whether activation of the BLA-ACC pathway affects the thermal sensitivity of hM3Dq-expressing mice, we performed a passive TPP task in the absence of a reward. All groups had low but comparable exploration of the hot and cold compartments (Figures S7I and S7J), although there was an emerging trend for lower time spent in the cold compartment of hM3Dq-expressing sham mice as compared with the controls. Importantly, BLA-ACC activation did not induce any locomotor adaptations (Figure S8B). Collectively, these data strongly point to a general involvement of the BLA-ACC pathway in CAAT behaviors and suggest that activity in this pathway may enhance the intrinsic aversive value of certain stimuli such as cold temperatures.

Depotentiation of BLA-ACC synapses in neuropathic pain mice reduces cold avoidance when facing approach-avoidance conflict

We reasoned that if neuropathy leads to BLA-ACC potentiation and if activity of this pathway is required for the expression of avoidance during conflicts, then depotentiating these synapses may normalize behavior.[43] We first sought to reverse the synaptic potentiation observed at BLA-ACC synapses *ex vivo*. Previous work has demonstrated experience-dependent increase of GluA2-lacking AMPARs in the amygdala, an effect that could be reversed by LFS.[44] We used a similar strategy and performed voltage-clamp recordings from ACC L2/3 pyramidal neurons obtained in slices from SNI mice while applying LFS of ChR2-expressing BLA terminals (Figure 4A). This led to long-term depression (LTD) of BLA-evoked EPSCs (Figure 4B) but did not induce changes in presynaptic release probability or coefficient of variation (Figures 4C and 4D). Given that we had observed both pre- and post-synaptic changes in SNI, we asked whether LFS-LTD at BLA-ACC L2/3 inputs involves a switch of AMPAR subunits. We voltage clamped the recorded neurons at different potentials before and after LTD induction and calculated the corresponding rectification index. Indeed, we observed that LFS-LTD was accompanied by a reduction of AMPAR rectification (Figure 4E), suggesting that pain-induced adaptations at this synapses could be reversed, at least partially, by LFS. We further sought to apply LFS at BLA-ACC inputs *in vivo* to probe whether it would be sufficient to reduce SNI mice's avoidance in the conflicting task (Figure 4F). LFS of ChR2-expressing BLA projections in the ACC (Figure 4G) 1 h prior to the task on day 7 of the training phase did not affect the time spent in the sucrose-associated compartment compared with the previous day for both control virus-expressing and ChR2-expressing SNI mice (Figures S9A and S9B), although it did increase the ChR2-expressing group's sucrose intake (Figure S9C). Furthermore, LFS stimulation increased SNI mice's preference score for the sucrose-associated compartment (Figure 4H) and increased the time spent in the licking zone (Figure 4I) and the sucrose intake (Figure 4J) when the temperature was 15°C, but not when it was 45°C (Figures S9D–S9F) without affecting overall locomotor activity (Figure S9G). LFS stimulation did not change the avoidance of the hot compartment in the TPP task (Figure S9H). However, it did increase the time that SNI-ChR2 mice spent in the cold compartment (Figure S9I), leaving the possibility that this manipulation increases the tolerance to cold temperatures,[30] contributing to the reduced avoidance in the conflicting task. In summary, these results indicate that LFS in a specific ACC subcircuit ameliorates aspects of pain behaviors.

DISCUSSION

Understanding the cellular and circuit mechanisms contributing to the complex negative symptoms occurring in the chronification of neuropathy is a crucial step for developing effective new treatments. Here, using an approach-avoidance task, we demonstrate that mice with chronic neuropathic and inflammatory, but not acute pain, favor avoidance of a cold environment over approaching a reward in a conflicting situation. This recapitulates in mice aspects of human pain-related fear-avoidance behaviors, which significantly contribute to the development and maintenance of chronic pain states.[45] We further find that, after nerve injury, an input- and cell-type-specific potentiation occurs in the ACC. This plasticity involves a switch of AMPAR subunits, increasing the relative contribution of GluA2-lacking AMPARs. LFS of BLA inputs in L2/3 of the ACC *ex vivo* induces LTD of excitatory transmission and resets AMPARs to a prepain state. Furthermore, chemogenetic activation of the BLA-ACC

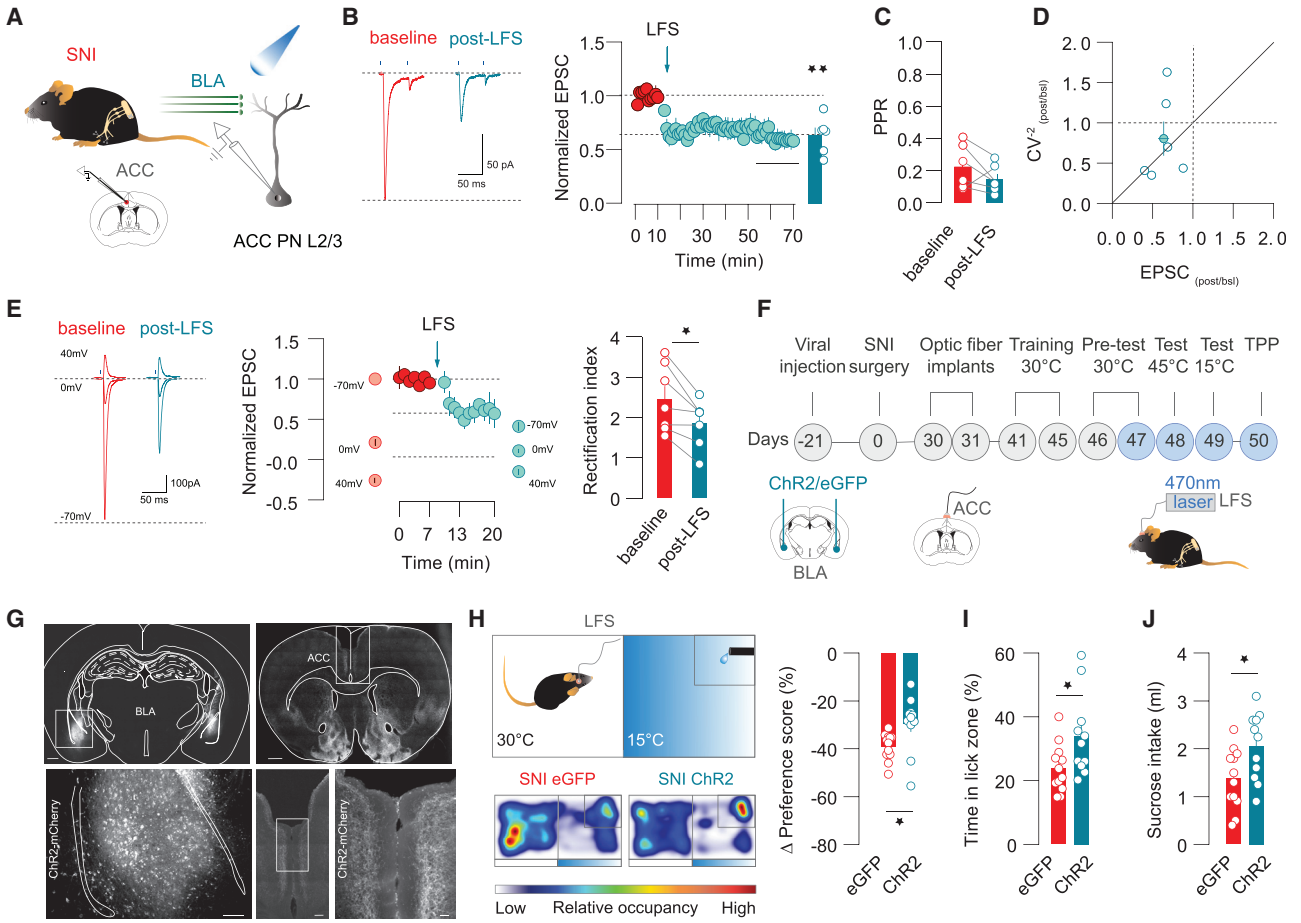

Figure 4. Low-frequency stimulation of BLA-ACC projections induces LTD of excitatory transmission *ex vivo* and reduces SNI mice's cold avoidance in the conflicting task *in vivo*

(A) Schematic of *ex vivo* recordings of L2/3 PNs of SNI mice in response to LFS of BLA terminals.

(B) Example traces, normalized EPSC vs. time plot, and bar graph with scatterplot showing LFS-LTD (indicated with arrow) of excitatory transmission at BLA-ACC L2/3 PNs synapses (N = 3 mice, n = 6 cells, 0.69 ± 0.08, baseline vs. post-LFS paired t test, $t_5 = 5.3$, **p = 0.003).

(C) Paired-pulse ratio of AMPAR-EPSCs before and after LFS-LTD at BLA-ACC L2/3 PNs (N = 3 mice, n = 6 cells, baseline vs. post-LFS 0.23 ± 0.06 vs. 0.15 ± 0.04, paired t test, $t_5 = 1.5$, p = 0.194).

(D) Coefficient of variation change (0.80 ± 0.2) vs. EPSC amplitude change (0.69 ± 0.08) after LFS-LTD. Open circles represent individual experiments, and filled circle represents the mean.

(E) Left: example traces showing AMPAR currents recorded at −70, 0, and 40mV. Middle: normalized EPSC recorded at 40, 0, and −70 mV before (red) and after (cyan) LFS-LTD induction (N = 4 mice, n = 7 cells, 0.52 ± 0.09, baseline vs. post-LFS paired t test, $t_6 = 5.51$, **p = 0.002). Right: rectification index before and after LFS-LTD, normalized to baseline EPSC recorded at −70 mV (2.46 ± 0.32 vs. 1.85 ± 0.22, baseline vs. LFS-LTD, paired t test, $t_6 = 3.451$, *p = 0.014).

(F) Schematics and timeline of viral injections, surgeries, and behavioral experiments.

(G) Example images showing expression of AAV2-CamKII-ChR2-mCherry in BLA and ACC as well as fiber optic placement site. Scale bar: 200 μm (top images) and 50 μm (bottom images).

(H) Left: cold test of the CAAT and heatmaps showing the relative time spent in the 30°C and 15°C compartments for SNI-EGFP (red) and SNI-ChR2 (cyan) mice. Right: difference of preference for the sucrose/15°C compartment from baseline (N = 12 vs. 11 mice, −38.89% ± 1.62% vs. −29.39% ± 3.51%, unpaired t test, $t_{21} = 2.528$, *p = 0.019).

(I) Percentage of time spent in lick zone of the cold compartment for SNI-EGFP and SNI-ChR2 mice (N = 12 vs. 11 mice, 23.88% ± 2.18% vs. 33.99% ± 3.84%, unpaired t test, $t_{21} = 2.341$, *p = 0.029).

(J) Sucrose intake during cold test for SNI-EGFP and SNI-ChR2 mice (N = 12 vs. 11 mice, 1.37 ± 0.18 mL vs. 2.05 ± 0.21 mL, unpaired t test, $t_{21} = 2.449$, *p = 0.023). Data are presented as mean ± SEM.

See also Figure S9.

projection induces avoidance in pain-free animals, while chemogenetic inhibition or LFS of the BLA-ACC projection *in vivo* rebalances approach-avoidance choices of neuropathic animals when facing conflicts.

Understanding the fine circuit and synaptic mechanisms in the ACC in chronic pain

The increased contribution of rectifying GluA2-lacking AMPARs to excitatory synaptic transmission in the BLA-ACC circuit is a

hallmark of plastic synaptic remodeling. These receptors, mainly composed of GluA1 subunits, are permeable to Ca^{2+} and shape synapses in an experience-dependent fashion.[42] Indeed, GluA1 subunits in the ACC L2/3 have been shown to underlie expression of long-term potentiation in an inflammatory pain model.[46,47] Furthermore, GluA1 plasticity occurs also in L5 pyramidal neurons following nerve injury, potentially at other inputs.[48] Blocking GluA1-containing receptors in the entire ACC have been shown to reduce sensitization,[48] highlighting the importance of these receptors for pain phenotypes. Our results are consistent with previous reports showing pre- and post-synaptic adaptations of excitatory transmission in ACC L2/3 pyramidal neurons in chronic pain conditions[49] and add a circuit-specific understanding of such synaptic modifications. Further, our experiments suggest that excitatory transmission at BLA-ACC interneuron synapses is not modified under neuropathic pain conditions, although plasticity of other projections may indirectly influence the total excitation/inhibition ratio. In contrast, pain states trigger selective strengthening of BLA inputs onto inhibitory neurons of the medial PFC (mPFC),[39,50] therefore reducing overall activity of projection neurons. Given the complexity of cortical inhibitory networks, more detailed work is needed to address potential pain-induced adaptations in diverse inhibitory subtypes. Additionally, it remains possible that parallel plasticity of NMDARs occurs at BLA-ACC synapses. Indeed, pain-induced plasticity of NMDARs in the ACC has extensively been reported in a synapse-specific and non-specific manner.[49,51]

BLA-ACC projection potentiation as an aversive signal facilitating avoidance

We speculate that the BLA provides a signal to the ACC, related to the emotional value of a stimulus rather than its sensory quality,[30] as we did not observe any change in allodynia behaviors when manipulating activity in this circuit. Indeed, other brain regions have been shown to be more relevant in the sensory coding of pain.[27,39] Importantly, SNI animals did not exhibit anhedonia behaviors at the examined time point after neuropathy induction, nor did they show alterations of reward seeking or thermal avoidance when granted a free choice. Instead, in our hands, pain animals displayed a reduced motivation for a reward only when forced to consume it in an aversive cold environment, consistent with previous results demonstrating that chronic pain animals have lower motivation to exert effort for a reward.[9] Furthermore, BLA-ACC chemogenetic inhibition did not affect approach or avoidance behaviors alone, suggesting that this circuit is not required for the purely motivational aspect of behavior but is rather involved in value-based decision-making. Previous studies have described other BLA projections in positive valence coding,[52,53] while a projection to the PFC shows correlated activity in response to aversion-predictive cues and facilitates fear behaviors.[29] Similarly to the PFC projection, our results are in line with a BLA-ACC circuit tuned to aversive coding, where the pain-induced synaptic potentiation could filter and enhance aversive representations. Importantly, our chemogenetic activation approach revealed a general role of this projection in conflict avoidance behaviors and suggests that pain states trigger converging mechanisms with other aversive states.

The selective strengthening of BLA inputs to ACC L2/3 pyramidal neurons may serve to modulate the gain of pyramidal neurons in L5[54] likewise contributing to top-down avoidance selection in a conflicting context.[55] However, as we did not observe synaptic modifications onto other ACC subpopulations receiving BLA inputs, it is unlikely that all BLA projections to the ACC encode negative valence in pain states. Importantly, as our approach for BLA-ACC inhibition could not be specific to a particular ACC layer, we could not disentangle the functional relevance specifically of the L2/3 projection. Nevertheless, global inhibition of this pathway reversed neuropathy animals' avoidance choices only when a conflict was present, suggesting its contribution in evaluating negative outcomes in uncertain situations.

We show that conflict-induced avoidance of mice with chronic pain is particularly present when cold was used as the aversive context. This result could be potentially due to the aversive value of the hot temperature for both pain and control mice. Indeed, the avoidance of control mice in the hot test was higher than in the cold one, while pain mice displayed similarly high avoidance for both temperatures. Notably, the activation of the BLA-ACC pathway in sham animals triggered avoidance of the cold but not the hot temperature. This observation suggests that the intrinsic aversive value of cold and hot stimuli may be processed through different mechanisms and circuits, accounting for the inconsistent effects observed when using hot temperatures. However, we do observe a small reduction of SNI mice's avoidance when we modulate the BLA-ACC projection, which may be explained by a partial contribution of this circuit to processing emotional responses to hot stimuli.

Understanding how circuit-specific activity patterns could improve pain states

Consistent with the idea that the ACC is an integrator of multimodal sensory and emotional information and a key orchestrator of value-based action selection,[19,22,34,49] we find that resetting activity at BLA-ACC synapses normalizes neuropathic pain animals' choices amid conflicting signals. Indeed, we demonstrate that LFS of BLA inputs to the ACC efficiently reduces the strength of excitatory transmission *ex vivo* as well as pain-avoidance behaviors *in vivo*. Importantly, such stimulation approaches have been successfully used to reverse synaptic plasticity adaptations and maladaptive behaviors in different disease states.[43] More recently, frequency stimulation strategies in the PFC and the ACC have been also proposed to alleviate pain behaviors.[56] However, in the latter study, high-frequency electrical stimulation in the ACC was more efficient to reduce pain-induced aversion.[56] These observations suggest that different projections to various ACC cell types may undergo distinct plasticity mechanisms, highlighting the importance of gaining a circuit-level understanding of pain-induced adaptations in the ACC. Finally, our data provide such circuit and synaptic mechanistic insights underlying specific aspects of pain behaviors and pave the way for developing new, more specific pain therapies.

Limitations of the study

Despite the importance of our findings, our study has some limitations. First, the design of our task included only one type of aversive context representing a somatosensory modality (hot/cold)

and only one type of reward (sucrose solution). It would be important to establish the generalizability of the BLA-ACC circuit in conflicts involving other sensory (e.g., loud noise, looming stimuli, predatory odor) and appetitive modalities (e.g., food, social reward, etc.). Second, we only used male mice in our investigation, which may obscure potential sex differences in pain-related behaviors. Third, we used an intraperitoneal (i.p.) injection of CNO for our chemogenetic approaches, which may also activate/inhibit potential collaterals of ACC-projecting BLA neurons, therefore contributing to the observed behavioral effects. However, the LFS that was applied specifically in the ACC supports the specificity of this pathway in the avoidance behavior. Finally, it would be important to follow the activity patterns of ACC-projecting BLA neurons during the different stages of the task in order to establish their exact contribution to the avoidance behavior.[57] All these points could represent potential new avenues for exploration.

STAR★METHODS

Detailed methods are provided in the online version of this paper and include the following:

- KEY RESOURCES TABLE
- RESOURCE AVAILABILITY
  - Lead contact
  - Materials availability
  - Data and code availability
- EXPERIMENTAL MODEL AND SUBJECT DETAILS
  - Mice
- METHOD DETAILS
  - Viruses
  - Optic fibers and instruments
  - Brain surgeries: Virus injections & optic fiber implants
  - Chronic neuropathic pain model: Spared nerve injury
  - Inflammatory pain model: Complete Freund Adjuvant
  - *Ex vivo* electrophysiology
  - Behavior
- QUANTIFICATION AND STATISTICAL ANALYSIS

SUPPLEMENTAL INFORMATION

Supplemental information can be found online at https://doi.org/10.1016/j.celrep.2023.113125.

ACKNOWLEDGMENTS

We thank the Nevian laboratory and Manuel Mameli for helpful discussions and feedback on the manuscript. We thank also Christian Dellenbach and Christian Käser for developing the custom-made drinking system. This work was supported by the Swiss National Science Foundation (T.N., grants 159872 and 182571) and the European Research Council (T.N., grant 682905).

AUTHOR CONTRIBUTIONS

Conceptualization, K.V. and T.N.; methodology, K.V. and T.N.; investigation, K.V.; writing – original draft, K.V.; writing – review & editing, K.V.; funding acquisition, T.N.; resources, M.A.A., N.R.N., and N.N.; supervision, T.N.

DECLARATION OF INTERESTS

The authors declare no competing interests.

Received: December 22, 2022
Revised: July 12, 2023
Accepted: August 28, 2023

REFERENCES

1. Kuner, R., and Flor, H. (2016). Structural plasticity and reorganisation in chronic pain. Nat. Rev. Neurosci. *18*, 20–30. https://doi.org/10.1038/nrn.2016.162.
2. Baliki, M.N., and Apkarian, A.V. (2015). Nociception, Pain, Negative Moods, and Behavior Selection. Neuron *87*, 474–491. https://doi.org/10.1016/j.neuron.2015.06.005.
3. Bushnell, M.C., Čeko, M., and Low, L.A. (2013). Cognitive and emotional control of pain and its disruption in chronic pain. Nat. Rev. Neurosci. *14*, 502–511. https://doi.org/10.1038/nrn3516.
4. Quartana, P.J., Campbell, C.M., and Edwards, R.R. (2009). Pain catastrophizing: a critical review. Expert Rev. Neurother. *9*, 745–758. https://doi.org/10.1586/ern.09.34.
5. Meulders, A. (2020). Fear in the context of pain: Lessons learned from 100 years of fear conditioning research. Behav. Res. Ther. *131*, 103635. https://doi.org/10.1016/j.brat.2020.103635.
6. Vlaeyen, J.W.S., Crombez, G., and Linton, S.J. (2016). The fear-avoidance model of pain. Pain *157*, 1588–1589. https://doi.org/10.1097/j.pain.0000000000000574.
7. Nees, F., and Becker, S. (2018). Psychological Processes in Chronic Pain: Influences of Reward and Fear Learning as Key Mechanisms - Behavioral Evidence, Neural Circuits, and Maladaptive Changes. Neuroscience *387*, 72–84. https://doi.org/10.1016/j.neuroscience.2017.08.051.
8. Price, D.D. (2000). Psychological and neural mechanisms of the affective dimension of pain. Science *288*, 1769–1772. https://doi.org/10.1126/science.288.5472.1769.
9. Schwartz, N., Temkin, P., Jurado, S., Lim, B.K., Heifets, B.D., Polepalli, J.S., and Malenka, R.C. (2014). Chronic pain. Decreased motivation during chronic pain requires long-term depression in the nucleus accumbens. Science *345*, 535–542. https://doi.org/10.1126/science.1253994.
10. Severeijns, R., Vlaeyen, J.W., van den Hout, M.A., and Weber, W.E. (2001). Pain catastrophizing predicts pain intensity, disability, and psychological distress independent of the level of physical impairment. Clin. J. Pain *17*, 165–172. https://doi.org/10.1097/00002508-200106000-00009.
11. Mankovsky, T., Lynch, M., Clark, A., Sawynok, J., and Sullivan, M.J. (2012). Pain catastrophizing predicts poor response to topical analgesics in patients with neuropathic pain. Pain Res. Manag. *17*, 10–14. https://doi.org/10.1155/2012/970423.
12. Boersma, K., and Linton, S.J. (2006). Expectancy, fear and pain in the prediction of chronic pain and disability: a prospective analysis. Eur. J. Pain *10*, 551–557. https://doi.org/10.1016/j.ejpain.2005.08.004.
13. Shackman, A.J., Salomons, T.V., Slagter, H.A., Fox, A.S., Winter, J.J., and Davidson, R.J. (2011). The Integration of Negative Affect, Pain, and Cognitive Control in the Cingulate Cortex. Nat. Rev. Neurosci. *12*, 154–167. https://doi.org/10.1038/nrn2994.
14. Apkarian, A.V., Bushnell, M.C., Treede, R.-D., and Zubieta, J.-K. (2005). Human brain mechanisms of pain perception and regulation in health and disease. Eur. J. Pain *9*, 463–484. https://doi.org/10.1016/j.ejpain.2004.11.001.
15. Blom, S.M., Pfister, J.-P., Santello, M., Senn, W., and Nevian, T. (2014). Nerve injury-induced neuropathic pain causes disinhibition of the anterior cingulate cortex. J. Neurosci. *34*, 5754–5764. https://doi.org/10.1523/JNEUROSCI.3667-13.2014.

16. Santello, M., and Nevian, T. (2015). Dysfunction of cortical dendritic integration in neuropathic pain reversed by serotoninergic neuromodulation. Neuron *86*, 233–246. https://doi.org/10.1016/j.neuron.2015.03.003.

17. Sellmeijer, J., Mathis, V., Hugel, S., Li, X.-H., Song, Q., Chen, Q.-Y., Barthas, F., Lutz, P.-E., Karatas, M., Luthi, A., et al. (2018). Hyperactivity of Anterior Cingulate Cortex Areas 24a/24b Drives Chronic Pain-Induced Anxiodepressive-like Consequences. J. Neurosci. *38*, 3102–3115. https://doi.org/10.1523/JNEUROSCI.3195-17.2018.

18. Zhao, R., Zhou, H., Huang, L., Xie, Z., Wang, J., Gan, W.-B., and Yang, G. (2018). Neuropathic Pain Causes Pyramidal Neuronal Hyperactivity in the Anterior Cingulate Cortex. Front. Cell. Neurosci. *12*, 107. https://doi.org/10.3389/fncel.2018.00107.

19. Rainville, P., Duncan, G.H., Price, D.D., Carrier, B., and Bushnell, M.C. (1997). Pain affect encoded in human anterior cingulate but not somatosensory cortex. Science *277*, 968–971. https://doi.org/10.1126/science.277.5328.968.

20. Urien, L., Xiao, Z., Dale, J., Bauer, E.P., Chen, Z., and Wang, J. (2018). Rate and Temporal Coding Mechanisms in the Anterior Cingulate Cortex for Pain Anticipation. Sci. Rep. *8*, 8298. https://doi.org/10.1038/s41598-018-26518-x.

21. Talmi, D., Dayan, P., Kiebel, S.J., Frith, C.D., and Dolan, R.J. (2009). How Humans Integrate the Prospects of Pain and Reward during Choice. J. Neurosci. *29*, 14617–14626. https://doi.org/10.1523/JNEUROSCI.2026-09.2009.

22. Monosov, I.E., Haber, S.N., Leuthardt, E.C., and Jezzini, A. (2020). Anterior cingulate cortex and the control of dynamic behavior in primates. Curr. Biol. *30*, R1442–R1454. https://doi.org/10.1016/j.cub.2020.10.009.

23. Umemoto, A., Lin, H., and Holroyd, C.B. (2023). Electrophysiological measures of conflict and reward processing are associated with decisions to engage in physical effort. Psychophysiology *60*, e14176. https://doi.org/10.1111/psyp.14176.

24. Meda, K.S., Patel, T., Braz, J.M., Malik, R., Turner, M.L., Seifikar, H., Basbaum, A.I., and Sohal, V.S. (2019). Microcircuit Mechanisms through which Mediodorsal Thalamic Input to Anterior Cingulate Cortex Exacerbates Pain-Related Aversion. Neuron *102*, 944–959.e3. https://doi.org/10.1016/j.neuron.2019.03.042.

25. Singh, A., Patel, D., Li, A., Hu, L., Zhang, Q., Liu, Y., Guo, X., Robinson, E., Martinez, E., Doan, L., et al. (2020). Mapping Cortical Integration of Sensory and Affective Pain Pathways. Curr. Biol. *30*, 1703–1715.e5. https://doi.org/10.1016/j.cub.2020.02.091.

26. Wang, Y.Q., Wang, J., Xia, S.H., Gutstein, H.B., Huang, Y.H., Schlüter, O.M., Cao, J.-L., and Dong, Y. (2021). Neuropathic pain generates silent synapses in thalamic projection to anterior cingulate cortex. Pain *162*, 1322–1333. https://doi.org/10.1097/j.pain.0000000000002149.

27. Zhu, X., Tang, H.-D., Dong, W.-Y., Kang, F., Liu, A., Mao, Y., Xie, W., Zhang, X., Cao, P., Zhou, W., et al. (2021). Distinct thalamocortical circuits underlie allodynia induced by tissue injury and by depression-like states. Nat. Neurosci. *24*, 542–553. https://doi.org/10.1038/s41593-021-00811-x.

28. Janak, P.H., and Tye, K.M. (2015). From circuits to behaviour in the amygdala. Nature *517*, 284–292. https://doi.org/10.1038/nature14188.

29. Burgos-Robles, A., Kimchi, E.Y., Izadmehr, E.M., Porzenheim, M.J., Ramos-Guasp, W.A., Nieh, E.H., Felix-Ortiz, A.C., Namburi, P., Leppla, C.A., Presbrey, K.N., et al. (2017). Amygdala inputs to prefrontal cortex guide behavior amid conflicting cues of reward and punishment. Nat. Neurosci. *20*, 824–835. https://doi.org/10.1038/nn.4553.

30. Corder, G., Ahanonu, B., Grewe, B.F., Wang, D., Schnitzer, M.J., and Scherrer, G. (2019). An amygdalar neural ensemble that encodes the unpleasantness of pain. Science *363*, 276–281. https://doi.org/10.1126/science.aap8586.

31. Becker, L.J., Fillinger, C., Waegaert, R., Journée, S.H., Hener, P., Ayazgok, B., Humo, M., Karatas, M., Thouaye, M., Gaikwad, M., et al. (2023). The basolateral amygdala-anterior cingulate pathway contributes to depression-like behaviors and comorbidity with chronic pain behaviors in male mice. Nat. Commun. *14*, 2198. https://doi.org/10.1038/s41467-023-37878-y.

32. Decosterd, I., and Woolf, C.J. (2000). Spared nerve injury: an animal model of persistent peripheral neuropathic pain. Pain *87*, 149–158. https://doi.org/10.1016/S0304-3959(00)00276-1.

33. Kragel, P.A., Kano, M., Van Oudenhove, L., Ly, H.G., Dupont, P., Rubio, A., Delon-Martin, C., Bonaz, B.L., Manuck, S.B., Gianaros, P.J., et al. (2018). Generalizable representations of pain, cognitive control, and negative emotion in medial frontal cortex. Nat. Neurosci. *21*, 283–289. https://doi.org/10.1038/s41593-017-0051-7.

34. Braem, S., King, J.A., Korb, F.M., Krebs, R.M., Notebaert, W., and Egner, T. (2017). The role of the anterior cingulate cortex in the affective evaluation of conflict. J. Cognit. Neurosci. *29*, 137–149. https://doi.org/10.1162/jocn_a_01023.

35. Fillinger, C., Yalcin, I., Barrot, M., and Veinante, P. (2017). Afferents to anterior cingulate areas 24a and 24b and midcingulate areas 24a' and 24b' in the mouse. Brain Struct. Funct. *222*, 1509–1532. https://doi.org/10.1007/s00429-016-1290-1.

36. Lee, J.-H.A., Miao, Z., Chen, Q.-Y., Li, X.-H., and Zhuo, M. (2021). Multiple synaptic connections into a single cortical pyramidal cell or interneuron in the anterior cingulate cortex of adult mice. Mol. Brain *14*, 88. https://doi.org/10.1186/s13041-021-00793-8.

37. Hosking, J.G., Cocker, P.J., and Winstanley, C.A. (2014). Dissociable Contributions of Anterior Cingulate Cortex and Basolateral Amygdala on a Rodent Cost/Benefit Decision-Making Task of Cognitive Effort. Neuropsychopharmacology *39*, 1558–1567. https://doi.org/10.1038/npp.2014.27.

38. Gao, Y.-J., Ren, W.-H., Zhang, Y.-Q., and Zhao, Z.-Q. (2004). Contributions of the anterior cingulate cortex and amygdala to pain- and fear-conditioned place avoidance in rats. Pain *110*, 343–353. https://doi.org/10.1016/j.pain.2004.04.030.

39. Huang, J., Gadotti, V.M., Chen, L., Souza, I.A., Huang, S., Wang, D., Ramakrishnan, C., Deisseroth, K., Zhang, Z., and Zamponi, G.W. (2019). A neuronal circuit for activating descending modulation of neuropathic pain. Nat. Neurosci. *22*, 1659–1668. https://doi.org/10.1038/s41593-019-0481-5.

40. Liu, S.J., and Zukin, R.S. (2007). Ca2+-permeable AMPA receptors in synaptic plasticity and neuronal death. Trends Neurosci. *30*, 126–134. https://doi.org/10.1016/j.tins.2007.01.006.

41. Xu, H., Wu, L.-J., Wang, H., Zhang, X., Vadakkan, K.I., Kim, S.S., Steenland, H.W., and Zhuo, M. (2008). Presynaptic and Postsynaptic Amplifications of Neuropathic Pain in the Anterior Cingulate Cortex. J. Neurosci. *28*, 7445–7453. https://doi.org/10.1523/JNEUROSCI.1812-08.2008.

42. Isaac, J.T.R., Ashby, M.C., and McBain, C.J. (2007). The Role of the GluR2 Subunit in AMPA Receptor Function and Synaptic Plasticity. Neuron *54*, 859–871. https://doi.org/10.1016/j.neuron.2007.06.001.

43. Creed, M., Pascoli, V.J., and Lüscher, C. (2015). Refining deep brain stimulation to emulate optogenetic treatment of synaptic pathology. Science *347*, 659–664. https://doi.org/10.1126/science.1260776.

44. Clem, R.L., and Huganir, R.L. (2010). Calcium-permeable AMPA receptor dynamics mediate fear memory erasure. Science *330*, 1108–1112. https://doi.org/10.1126/science.1195298.

45. Zale, E.L., and Ditre, J.W. (2015). Pain-Related Fear, Disability, and the Fear-Avoidance Model of Chronic Pain. Curr. Opin. Psychol. *5*, 24–30. https://doi.org/10.1016/j.copsyc.2015.03.014.

46. Toyoda, H., Zhao, M.-G., Ulzhöfer, B., Wu, L.-J., Xu, H., Seeburg, P.H., Sprengel, R., Kuner, R., and Zhuo, M. (2009). Roles of the AMPA receptor subunit GluA1 but not GluA2 in synaptic potentiation and activation of ERK in the anterior cingulate cortex. Mol. Pain *5*, 46. https://doi.org/10.1186/1744-8069-5-46.

47. Toyoda, H., Wu, L.-J., Zhao, M.-G., Xu, H., and Zhuo, M. (2007). Time-dependent postsynaptic AMPA GluR1 receptor recruitment in the cingulate synaptic potentiation. Dev. Neurobiol. *67*, 498–509. https://doi.org/10.1002/dneu.20380.

48. Chen, T., Wang, W., Dong, Y.-L., Zhang, M.-M., Wang, J., Koga, K., Liao, Y.-H., Li, J.-L., Budisantoso, T., Shigemoto, R., et al. (2014). Postsynaptic insertion of AMPA receptor onto cortical pyramidal neurons in the anterior cingulate cortex after peripheral nerve injury. Mol. Brain *7*, 76. https://doi.org/10.1186/s13041-014-0076-8.

49. Bliss, T.V.P., Collingridge, G.L., Kaang, B.-K., and Zhuo, M. (2016). Synaptic plasticity in the anterior cingulate cortex in acute and chronic pain. Nat. Rev. Neurosci. *17*, 485–496. https://doi.org/10.1038/nrn.2016.68.

50. Ji, G., Sun, H., Fu, Y., Li, Z., Pais-Vieira, M., Galhardo, V., and Neugebauer, V. (2010). Cognitive Impairment in Pain through Amygdala-Driven Prefrontal Cortical Deactivation. J. Neurosci. *30*, 5451–5464. https://doi.org/10.1523/JNEUROSCI.0225-10.2010.

51. Hogrefe, N., Blom, S.M., Valentinova, K., Ntamati, N.R., Jonker, L.J.E., Nevian, N.E., and Nevian, T. (2022). Long-Lasting, Pathway-Specific Impairment of a Novel Form of Spike-Timing-Dependent Long-Term Depression by Neuropathic Pain in the Anterior Cingulate Cortex. J. Neurosci. *42*, 2166–2179. https://doi.org/10.1523/JNEUROSCI.0326-21.2022.

52. Beyeler, A., Namburi, P., Glober, G.F., Simonnet, C., Calhoon, G.G., Conyers, G.F., Luck, R., Wildes, C.P., and Tye, K.M. (2016). Divergent Routing of Positive and Negative Information from the Amygdala during Memory Retrieval. Neuron *90*, 348–361. https://doi.org/10.1016/j.neuron.2016.03.004.

53. Beyeler, A., Chang, C.-J., Silvestre, M., Lévêque, C., Namburi, P., Wildes, C.P., and Tye, K.M. (2018). Organization of Valence-Encoding and Projection-Defined Neurons in the Basolateral Amygdala. Cell Rep. *22*, 905–918. https://doi.org/10.1016/j.celrep.2017.12.097.

54. Quiquempoix, M., Fayad, S.L., Boutourlinsky, K., Leresche, N., Lambert, R.C., and Bessaih, T. (2018). Layer 2/3 Pyramidal Neurons Control the Gain of Cortical Output. Cell Rep. *24*, 2799–2807.e4. https://doi.org/10.1016/j.celrep.2018.08.038.

55. Duque, J., Olivier, E., and Rushworth, M. (2013). Top-down inhibitory control exerted by the medial frontal cortex during action selection under conflict. J. Cognit. Neurosci. *25*, 1634–1648. https://doi.org/10.1162/jocn_a_00421.

56. Liu, Y., Xu, H., Sun, G., Vemulapalli, B., Jee, H.J., Zhang, Q., and Wang, J. (2021). Frequency Dependent Electrical Stimulation of PFC and ACC for Acute Pain Treatment in Rats. Front. Pain Res. *2*, 728045.

57. Acuña, M.A., Kasanetz, F., De Luna, P., Falkowska, M., and Nevian, T. (2023). Principles of nociceptive coding in the anterior cingulate cortex. Proc. Natl. Acad. Sci. USA *120*, e2212394120. https://doi.org/10.1073/pnas.2212394120.

58. Smith, M.L., Asada, N., and Malenka, R.C. (2021). Anterior cingulate inputs to nucleus accumbens control the social transfer of pain and analgesia. Science *371*, 153–159. https://doi.org/10.1126/science.abe3040.

STAR★METHODS

KEY RESOURCES TABLE

REAGENT or RESOURCE	SOURCE	IDENTIFIER
Bacterial and virus strains		
AAV2-CaMKIIa-hChR2-(H134R)-eYFP	VVF	v661
AAV2-CaMKIIa-hChR2-(H134R)-mCherry	VVF	v204-1
AAV-retro2-hSyn1-eBFP2-iCre-WPRE-hGHp(A)	VVF	v148
AAV-retro2-hSyn1-chI-mCherry-2A-iCre-WPRE-SV40p(A)	VVF	v147
AAV-retro2-hSyn1-chI-EGFP-T2a-iCre	VVF	v146
AAV2-hSyn1-dlox-HA-hM4D(6F)-mCitrine	VVF	v93
AAV2-hSyn1-dlox-hM3D(Gq)-mCherry(rev)-dlox	VVF	v89
AAV1-CAG-flex-tdTomato-WPRE-bGH	VVF	v167
AAV1/2-hsyn-DIO-eGFP-WPRE-hGHp(A)	VVF	v115
AAV2-mCaMKIIa-eGFP-WPRE-hGHp(A)	VVF	v113
AAV8-CaMKII-Cre-mCherry	UNC	AV5054b
rAAV1-*syn*-DIO-TVA-RG-eGFP	UNC	
EnVA-DG-Rabies-mCherry	Salk Institute	
Chemicals, peptides, and recombinant proteins		
Complete Freund's Adjuvant (CFA)	Aviva Systems Biology	Cat#OORA00327
Clozapine-*N*-Oxide (CNO)	Tocris	Cat#6329
Alexa Fluor 405 Streptavidin	Thermo Fischer	Cat#S32351
Alexa Fluor 488 Streptavidin	Thermo Fischer	Cat#S11223
Alexa Fluor 594 Streptavidin	Thermo Fischer	Cat#S11227
Paraformaldehyde (PFA)	Sigma Aldrich	Cat#1004960700
Triton X-100	Sigma Aldrich	Cat#X100-100ML
Mowiol 4-88	Sigma Aldrich	Cat#81381-50G
Experimental models: Organisms/strains		
C57Bl/6J	Janvier Labs	C57Bl/6J
Vgat-ires-Cre	Janvier Labs	Vgat-ires-Cre
Software and algorithms		
MATLAB	MathWorks	N/A
Igor Pro	WaveMetrics	N/A
Graphpad Prism	Dotmatics	N/A

RESOURCE AVAILABILITY

Lead contact

Further information and requests for resources and reagents should be directed to and will be fulfilled by the lead contact, Thomas Nevian (thomas.nevian@unibe.ch).

Materials availability

This study did not generate new unique reagents.

Data and code availability

- All data reported in this paper will be shared by the lead contact upon request.

- This paper does not report original code.
- Any additional information required to reanalyze the data reported in this paper is available from the lead contact upon request.

EXPERIMENTAL MODEL AND SUBJECT DETAILS

Mice

All procedures aimed to fulfill the criterion of the 3Rs and were approved by the Veterinary Offices of the canton of Bern (Switzerland; license BE 133/16). Adult (4–12 weeks) male C57BL/6J wild-type or Vgat-ires-Cre mice (Janvier Labs) were group-housed (three to five per cage) on a 12–12 h light cycle (lights on at 7:00) with food and water *ad libitum*.

METHOD DETAILS

Viruses

Viral vectors were obtained from University of North Carolina Vector Core, Chapel Hill, USA, Salk Institute viral vector core, USA or Viral Vector Facility, Neuroscience Center Zurich, Switzerland. 200-300nL of AAV2-CaMKIIa-hChR2-(H134R)-eYFP or AAV2-CaMKIIa-hChR2-(H134R)-mCherry was infused into the basolateral amygdala (BLA, anterior–posterior (AP): −1.35 mm; medial–lateral (ML): ±3.25 mm; dorsal-ventral (DV): −4.75 mm from bregma) in the right hemisphere of C57BL/6 mice for assessing input-specific synaptic adaptations in the ACC *ex vivo*. Vgat-ires-Cre mice were unilaterally injected with AAV1-CAG-flex-tdTomato-WPRE-bGH in the anterior cingulate cortex (ACC, AP: +1 mm; ML: ±0.3 mm; DV: −1.75 mm from bregma) for targeted GABA neurons recordings. For rabies-tracing, animals were injected with AAV8-CaMKII-Cre-mCherry and rAAV1-*syn*-DIO-TVA-RG-eGFP (UNC) in the right hemisphere ACC and 15 days after with EnVA-ΔG-Rabies-mCherry (Salk Institute), animals were then perfused a week after. For chemogenetic inhibition during behavioral experiments, mice were bilaterally injected with AAVretro2-hSyn1-eBFP2-iCre-WPRE-hGHp(A) or AAVretro2-hSyn1-chl-mCherry-2A-iCre-WPRE-SV40p(A) in the ACC and AAV1-CAG-flex-tdTomato-WPRE-bGH or AAV1/2-hSyn1-DIO-eGFP-WPRE-hGHp(A) in the BLA as control or with AAV2-hsyn-dlox-HA-hM4D(6F)-mCitrine in the BLA for AAC-projecting BLA neurons inhibition. For chemogenetic excitation experiments, mice were bilaterally injected with ssAAVretro2-hSyn1-chl-EGFP-T2a-iCre in the ACC and with ssAAV-2/2-hSyn1-dlox-hM3D(Gq)-mCherry(rev)-dlox in the BLA. For optogenetic manipulation during behavioral experiments, mice were bilaterally injected with AAV2-mCaMKIIα-eGFP-WPRE-hGHp(A) in the BLA as control and with AAV2-CaMKIIa-hChR2(H134R)-mCherry in the BLA for low-frequency stimulation-induced depotentiation.

Optic fibers and instruments

Custom designed dual optic fiber cannulas (1.5mm of length) with guiding socket and a pitch of 0.6mm between the two fibers (Doric Lenses, Canada) were implanted over the ACC of mice and connected to a 473nm wavelength laser (MBL-FN-473/1∼100mW, Changchun New Industries Optoelectronics Technology Co., Ltd) via a guiding socket to SMA fiberoptic patchcord (Doric Lenses). Some of the animals were bilaterally implanted with in house-prepared optic fibers (FT22EMT, Thor Labs) cleaved with a fiber optic carbide scribe (F19773, Fiber Instrument Sales) at 7.8mm of length inserted and glued with Uhu Plus glue into two ceramic ferrule cannulas (6 mm length, LMFL-230-NN-C35 LC/MU MM, Senko Advanced Components). The fibers were then polished with different fiber polishing sheets (Thor Labs). Once implanted, the ferrules were connected to the laser via an intensity division splitter (DMC_1x2i_VIS_FC, Doric Lenses) connected to two FCM to ZF1.25 fiberoptic patchcords (Doric Lenses) and an FC/PC to SMA patch cable (Thor Labs). The laser was connected to an in house-built laser controller (Electronic workshop, University Bern) which was set to deliver 5 min stimulation at 1 Hz with a duration of 10ms.The laser output power at the end of the fiber optics was set to ∼10mW.

Brain surgeries: Virus injections & optic fiber implants

All surgeries were conducted under aseptic conditions with glass bead sterilized surgical tools (Fine Science Tools). Adult mice of at least 4–5 weeks of age were anesthetized with isoflurane (2% induction, 1.5% maintenance) vaporized with 100% oxygen and placed on a stereotaxic frame (Stoelting, USA). Eye ointment (Pharma Medica AG, Rogwil, Switzerland) was applied and body temperature was monitored and maintained at 35°C–37°C using a heating pad (Harvard Apparatus). A mix of analgesics and anti-inflammatory reagents was subcutaneously injected (Dexamethasone, 2 mg/kg; Carprofen 5 mg/kg). After removing the hair and cleaning the area of the head with antiseptics, a local anesthetic (lidocaine) was injected under the skin over the skull, a longitudinal incision was made along the head's skin and a small craniotomy was performed over the BLA or the ACC. Uni or bilateral injections of 200–300 nL of virus were performed at the desired coordinates through a glass micropipette (5μL, BlauBrand micropipettes, intraMARK) attached to a standard holder at a rate of approximately 100 nL min^{-1} using an air pressure system (Picospritzer II, Parker Hannifin,NH,US). The injection pipette was withdrawn from the brain shortly after the infusion. Finally, the skin was sutured with an absorbable thread (4-0 coated VICRYL rapid suture, Ethicon). For optic fiber implants, the skin above the skull was incised and glued to the borders of the skull via tissue adhesive (Vetbond). The surface of the skull was scratched with a blade and a craniotomy was performed above the ACC at AP: 1mm, ML: 0.3mm and DV: −1.5mm from bregma when the dual optic fiber cannula with a guiding socket was used and at AP: 1mm, ML: 0.56mm and DV: −1.52mm and under a 15° angle when the ceramic ferrule cannulas were used. The cannulas were guided and inserted inside the brain and secured in place with a light curable dental cement (Tetric

EvoFlow). A micro screw was inserted in the skull for additional stability of the implant and the whole skull area was covered with dental cement. Animals were allowed to recover from the surgery and were weight-checked and injected with a cocktail of analgesics and anti-inflammatory every day for few days.

Chronic neuropathic pain model: Spared nerve injury

One-two weeks after brain surgeries, animals were anesthetized with isofluorane (1.5%) and placed under a sterilized fume hood for spared nerve injury (SNI) or a sham operation, which was always performed on the left hind paw. A small incision in the left thigh was made to expose the sciatic nerve and a silk thread (12x18″ 45cm, Sofsilk) was used to make two consecutive loose ligations around the peroneal and tibial nerve branch, which was then cut posterior to the ligation leaving the sural nerve branch intact. For sham surgery the sciatic nerve was exposed but not ligated. The skin was then sutured (4-0 coated VICRYL rapid suture, Ethicon) and disinfected with Betadine. Animals did not receive analgesics following the surgery but were monitored for a few days after.

Inflammatory pain model: Complete Freund Adjuvant

Animals were briefly anesthetized with isofluorane (2%) and a 30μL of the inflammatory agent Complete Freund Adjuvant (CFA) was injected in the plantar surface of the left hind paw of mice. As control, other mice were injected with the same volume of saline solution.

Ex vivo electrophysiology

SNI or Sham animals (10–50 days after surgery) were anesthetized with isofluorane (3%) for preparation of ACC-containing brain slices. The brain was removed and slicing was done in bubbled ice-cold 95% O_2/5% CO_2-equilibrated solution containing (in mM): 110 choline chloride, 25 glucose, 25 $NaHCO_3$, 7 $MgCl_2$, 116 ascorbic acid, 3.1 sodium pyruvate, 2.5 KCl, 1.25 NaH_2PO_4, and 0.5 $CaCl_2$ and ACC-containing coronal slices (250 μm) were obtained using a vibration microtome (Microm, Thermo scientific).The slices were then transferred for 10 min to warmed solution (34°C) in 95% O_2/5% CO_2-equilibrated artificial cerebrospinal fluid containing (in mM): 124 NaCl, 26.2 $NaHCO_3$, 11 glucose, 2.5 KCl, 2.5 $CaCl_2$,1.3 $MgCl_2$, and 1 NaH_2PO_4. Patch-clamp recordings (flow rate of 2.5 mL min^{-1} of bath solution) were obtained under an Olympus-BX51WI microscope equipped with an IR CCD camera (Photometrics, Cool SNAP, ES^2) at 32°C and using borosilicate glass pipettes (75mm long, 2mm outside diameter, 0.5mm wall resistance: 5–8 MΩ; Hilgenberg, Germany) pulled with a vertical puller (Narishige PC-100, Japan). Currents were amplified, filtered at 5 kHz and digitized at 10 kHz using an amplifier (Dagan BVC-700A, Cornerstone series) with an ITC-18 board (Instrutech, HEKA Instruments) and IgorPro software (Wavemetrics). Access resistance was monitored by a step of −5 mV (0.1 Hz) and experiments were discarded if it was increasing more than 20% throughout the experiment. Recordings were made in voltage-clamp configuration from layer 2/3, layer 5 pyramidal or identified GABA (Vgat-cre mice expressing Cre-dependent tdTomato) or in current-clamp mode from BLA neurons (expressing DREADDi). For AMPA/NMDA, AMPA/GABA ratios, rectification properties, long-term plasticity and paired pulse ratio measurements the internal solution contained (in mM): 125 gluconic acid, 130 CsOH, 5 CsCl, 10 Na-phosphocreatine, 4, Mg-ATP, 0.3 Na-GTP, 10 HEPES, 0.1 spermine, and 5 QX-314. For current-clamp experiments the internal solution contained (in mM): 115 K-gluconate, 20 KCl, 2 ATP-Mg, 2 ATP-Na_2, 10 Na creatine-phosphate, 0.3 GTP, 10 HEPES. All internal solutions contained biocytin (2 mg/ml) and all slices with recorded biocytin-filled neurons were reconstructed. For determining the AMPAR/NMDAR ratios at BLA to ACC synapses, EPSCs were evoked from ChR2-expressing BLA axons with a single 470nm, 5ms light pulse using an LED illumination system (Thor Labs) over the slice and through a 40x objective. A mixture of AMPA and NMDA currents were evoked at +40 mV (in the presence of Gabazine or TTX (1μM) and 4-AP (0.5mM)) or at −70mV and +40mV, respectively. The two components were pharmacologically isolated by adding 2-amino-5-phosphonovaleric acid (APV, 50μM) in the recording solution and by subsequent identification of the individual currents via digital subtraction. For AMPA/GABA ratios, EPSCs were evoked at −70mV and IPSCs at 10mV in presence of APV and pharmacologically validated by adding gabazine (10μM). The rectification index was computed by recording pharmacologically isolated AMPA-EPSCs at −70 mV, 0mV and +40 mV and was calculated as follows: (AMPA-EPSC at −70/AMPA-EPSC at +40)/1.75. Because of the liquid junction potential, the current recorded at 0mV was non-zero. For better visual representation of the I/V curves, we calculated the percent contribution of this current for each cell to the component recorded at +40mV and −70mV and we subtracted it, after what the currents at 0mv and 40mV were normalized to the one recorded at −70mV. To assess presynaptic release properties, trains (5 pulses at 5 Hz) of AMPAR-EPSCs were evoked by activating ChR2-expressing axons as mentioned above. The amplitudes of EPSC trains were normalized to the amplitude of the first pulse. To assess the contribution of GluA2-lacking AMPARs we recorded BLA-evoked and AMPA-mediated EPSCs at −70mV. After a baseline of 10min the selective GluA2-lacking AMPAR antagonist 1-Naphthylacetyl spermine trihydrochloride (NASPM, 20μM) was applied on slices from Sham and SNI mice and its effect was recorded for at least 15min after application. For the *ex vivo* validation of hMD4i-expressing BLA neurons, recordings were performed in visually identified and posthoc-validated BLA neurons in the current-clamp mode. A series of increasing (−50pA–350pA with 50pA increments), 600ms-long current steps were delivered to determine the neuronal input-output function before and after application of the hM4Di agonist Clozapine-N-Oxyde (CNO, 5μM), as a measure of intrinsic excitability. To determine the input resistance, the cells were hyperpolarized by injection of a −300 pA current pulse of 100 ms duration. For long-term plasticity experiments, pharmacologically isolated AMPA-mediated EPSCs were recorded in ACC layer 2/3 neurons from SNI mice in response to ChR2-expressing BLA terminal stimulation. After a baseline of about 10min, low-frequency stimulation (2 paired pulses @ 50Hz delivered @ 1Hz for 5min, 5ms pulse duration) was applied and EPSCs were monitor an hour after. The paired-pulse ratio was calculated as the ratio of the second EPSC/first EPSC. The coefficient of variation was calculated as follows: $CV^{-2} = \mu 2/\sigma 2$

with μ being the mean amplitude of the EPSC and $\sigma 2$ its variance. For determining the rectification of AMPARs before and after LFS-LTD, we recorded AMPA-mediated EPSCs at +40mV, 0mV and −70mV in ACC layer 2/3 from SNI mice, then after a short baseline (7min, at −70mV) we applied the LFS and monitored AMPA-EPSC for about 13–15 min, after what we performed again recordings at 0mV and 40mV. The rectification index was calculated as mentioned above.

Behavior

Von Frey

Mice were put to habituate for 10–20 min in a custom-made plexiglas enclosure (10 cm × 10 cm) placed on a grid. Mechanical allodynia was assessed using an electronic Von Frey anesthesiometer (IITC Life Science) by slowly applying pressure to the midplantar surface of the hind-paw with a Von Frey filament until a paw withdrawal was evoked and the corresponding stimulation strength was recorded (in grams). For each mouse six independent measures of the left (Sham/SNI-injured or Saline/CFA-injected) and the right (uninjured) hind paw were taken with an interval between each measurement of about 2–3 min. The measurements were averaged before and 10, 20, 30 and 40 days after Sham/SNI surgery or before, 24h and 1 week after Saline/CFA injection. For chemogenetic manipulation experiments, all mice received a Clozapine-N-Oxyde (CNO, 10 mg/kg) injection 20–30 min prior von Frey testing on day 40 after Sham/SNI surgery.

Thermal stimulation-induced coping behavior

Mice were put to habituate for 10–20 min in a custom-made plexiglas enclosure (10 cm × 10 cm) placed on a grid. The left hind paw was approached with a 1mL syringe containing hot water (temperature ∼70°C–80°C) or acetone (cold stimulation) and a drop was ejected on the lower surface of the paw until a reaction was produced. Typical coping reactions included increased velocity (escape), licking, paw flinches, prolonged paw lifting and escape jumps. The behavior was videotaped and the total time spent coping was manually scored. For chemogenetic manipulation experiments, all mice received a thermal stimulation (hot and cold) before and 20–30 min after CNO (10 mg/kg) injection.

Sucrose preference test

The sucrose preference test was performed with one Sham or SNI mouse per cage (40 days after surgery), with free access to two bottles of 1% sucrose for 2 consecutive days. On day 3 and 4 (test day) mice were exposed for 48 h to two bottles, one filled with 1% sucrose and the other one with drinking water. The sucrose preference was defined as the average ratio of the consumption of sucrose solution vs. total intake (sucrose + water) during the test.

Thermal gradient track

Sham and SNI mice (40 days after surgery) were exposed for 1 h to a linear thermal gradient track (L 121.92 cm x W 8.25 cm x H 15.24 cm, BioSep) with temperature zones varying from 8°C to 46°C. The thermal gradient was obtained by placing the two ends of the linear track on a hot and a cold plate respectively. The luminosity of the room was set to 10 lux to ensure exploration. The video tracking of the mice was performed during the second half hour and the time spent in each thermal zone was computed with the BioSep Thermal gradient test software.

Thermal place preference

A plastic box (17 cm × 33 cm) divided into two equal compartments by a plastic separator was placed on top of two thermal plates (16 cm × 16 cm each, BioSep) positioned next to each other, creating two arenas of 8 cm × 32 cm each, where two animals could be video tracked in parallel. One plate was set to 30°C and the other one to either 45°C or 15°C. Sham and SNI mice (around 50 days after surgery) were placed in the arena for 10 min and were allowed to freely explore the comfortable (8 × 16cm) and the hot/cold (8 × 16cm) plates. Videos were acquired using Ethovision, Noldus and the analysis of the relative time spent in each compartment was computed by a custom-written MATLAB script and expressed in percentage. For chemogenetic and optogenetic manipulation experiments, mice received a CNO (10 mg/kg) injection or low frequency stimulation (1Hz, 5min) 30 min and ∼1 h prior behavioral testing respectively.

Conflicting approach-avoidance task

C57BL/6J male mice underwent Sham and SNI surgery. For chemogenetic and optogenetic experiments, mice received viral injections 2–3 weeks prior to Sham/SNI surgery. The mechanical sensitivity of the left and right paws was measured with the von Frey test before and 10, 20, 30 and 40 days post-surgery (control and chemogenetic groups) and before, 24h and 7 days after Saline/CFA injection (for inflammatory pain group). All animals were housed according to their treatment to avoid potential social transfer of pain.[58] Animal's weight and well-being were regularly monitored throughout the development of chronic pain. For optogenetic experiments, mice were implanted with optic fibers around 30 days after Sham/SNI surgery. 40 days after Sham/SNI surgery all mice were water-deprived for 12 h and were put immediately after to habituate for 15 min per day during seven consecutive days, with 12 h-water deprivation periods between each day, in an arena (16 cm × 32 cm) divided into two equal compartments (16 cm × 16 cm). The temperature of the floor of each compartment could be controlled by using two thermal plates positioned next to each other (BioSep). For this habituation phase (7 days) the temperature of both plates was set to 30°C. Access to 10% sucrose solution was available in the corner of one of the compartments using an in house-built sucrose delivery lick system (Electronic workshop, University Bern). For chemogenetic manipulation experiments, all animals received a mock i.p poke with a needle 20–30 min before being allowed to freely explore the arena and to drink the sucrose solution in the first five days of the training in order to habituate them to being grabbed and injected. The relative time spent in the sucrose associated compartment and the sucrose licking zone were taken as a metric for mice's preference for this compartment and were calculated as follows:

$$sucrose\ preference\ for\ each\ day\ =\ \frac{time\ spent\ in\ the\ sucrose\ compartment\ for\ that\ day}{total\ time}x100$$

or

$$lick\ zone\ preference\ for\ each\ day\ =\ \frac{time\ spent\ in\ lick\ zone\ for\ that\ day}{total\ time}x100$$

Animals that spent on average less than 50% of the time in the sucrose-associated compartment during the training period were excluded from the analysis (2 Sham and 1 SNI mice from the chemogenetic group of animals). Then they received a saline injection on day 6 and a CNO (10 mg/kg) injection on day 7 in order to probe a potential effect of a liquid or CNO on mice's preference for the sucrose-associated compartment. Video tracking and analysis were obtained with Ethovision, Noldus. For optogenetic experiments, mice were habituated to being restrained for tethering during the first six days of the training and were actually tethered and received low-frequency stimulation (1Hz, 5 min) $\sim$ 1 h prior exposure to the arena on day 7 to probe whether the stimulation would impact animals' preference. For inflammatory pain animals the Saline/CFA injection was performed 10–15 min prior introducing the mice to the arena on the last day of the training (day 7). There was no significant difference between mice's preference on day 6 and day 7 across all groups, regardless of the treatment. The habituation training was sufficient to reliably learn the location of the water spout and to consume the sucrose solution according to each mouse's preference. To set the baseline preference of mice for the sucrose compartment, their relative time spent in the sucrose associated compartment was averaged for the last two days of the training:

$$baseline\ sucrose\ preference\ =\ \frac{sucrose\ preference\ on\ day\ 6+sucrose\ preference\ on\ day\ 7}{2}$$

On day 8 and day 9 after training, animals were placed in the same arena, but this time the floor of the sucrose-associated compartment was set to 45°C and 15°C respectively. The relative time spent in the sucrose-associated compartment on test days 8 and 9 was subtracted from the baseline preference (day6+ day7) to obtain the test preference score for the hot and cold temperatures respectively:

$$\Delta\ preference\ score\ =\ sucrose\ preference\ day\ 8\ (or\ 9)\ -\ baseline\ preference$$

Additional analysis of the total sucrose consumption for each day was performed. All animals from all groups (control, chemogenetic and optogenetic) underwent thermal place preference test (as described above) after the conflicting approach avoidance task and 10 days later only control Sham/SNI, Saline/CFA and chemogenetic groups received thermal stimulation (hot water or acetone drop on the injured hind paw) for affective coping scoring. Animals from the chemogenetic and optogenetic groups were perfused after behavioral testing and their brains were sliced and verified for correct viral expression in the target areas and correct implantation of the optic fibers. Misinjected or misimplanted animals were discarded from the behavioral analysis. For Saline/CFA mice the behavior was performed as described above with the difference that animals were first trained for 6 consecutive days to the arena with comfortable temperature of the floor and free access to sucrose solution and on day 7 of the training received randomly either Saline or CFA injection of the left hind paw. The following day (24h post-injection) all mice were submitted to the hot conflict test followed by a von Frey test and the next day (48h post-injection) to the cold conflict test. The animals were submitted again to the hot test 6 days after Saline/CFA injection and to the cold test 7 days post-injection followed by von Frey test. On day 8 after Saline/CFA injection all animals underwent thermal stimulation with hot water and acetone for affective coping scoring.

Histology and immunofluorescence

Animals used for behavioral experiments with chemogenetic or optogenetic manipulation were perfused with 4% PFA and the brains were stored in PFA for 1–2 days before slicing. Slices (100μm) were obtained using a Leica VT1000S vibratome and mounted with Mowiol on microscopy slides before imaging. Brain slices used for electrophysiological recordings were fixed in 4% PFA at 4°C overnight for reconstruction. After washing the slices with PBS (3× for 10 min), they were permeabilized in PBS containing 2% Triton X-100 for 1 h. Then slices were incubated with streptavidin-conjugated Alexa 488/Alexa 594/Alexa 405 (1:200; Invitrogen) in PBS containing 1% Triton X-100 depending on the fluorescence tag. After washing with PBS (3× for 10 min), the processed slices were embedded in Mowiol on microscopy slides. Fluorescently labeled coronal brain slices were imaged using a confocal microscope (Leica Microsystems, SP8) equipped with a white-light laser and two GaAsP-detectors (HyD). Imaging was performed with a 20× objective (Leica Microsystems, HC PL APO, 20×, NA 0.75 IMM CORR CS2) from the rostral ACC. The region containing the labeled pyramidal or GABA neuron was imaged in the tile-scan mode.

QUANTIFICATION AND STATISTICAL ANALYSIS

Data were analyzed using custom-written IGOR procedures. The program Prism (GraphPad) was used for statistical analysis, and data were tested with paired or unpaired Student's t test, or with one- or two-way ANOVA together with Sidak correction for multiple comparisons. Statistical significance was asserted for $p < 0.05$. Data are expressed as mean ± SEM. Testing was always performed two-tailed with $\alpha = 0.05$.